Deltares

Enabling Delta Life

The effect of erosion-resistant layers in the subsurface on the morphological evolution of the schematized Ameland inlet system

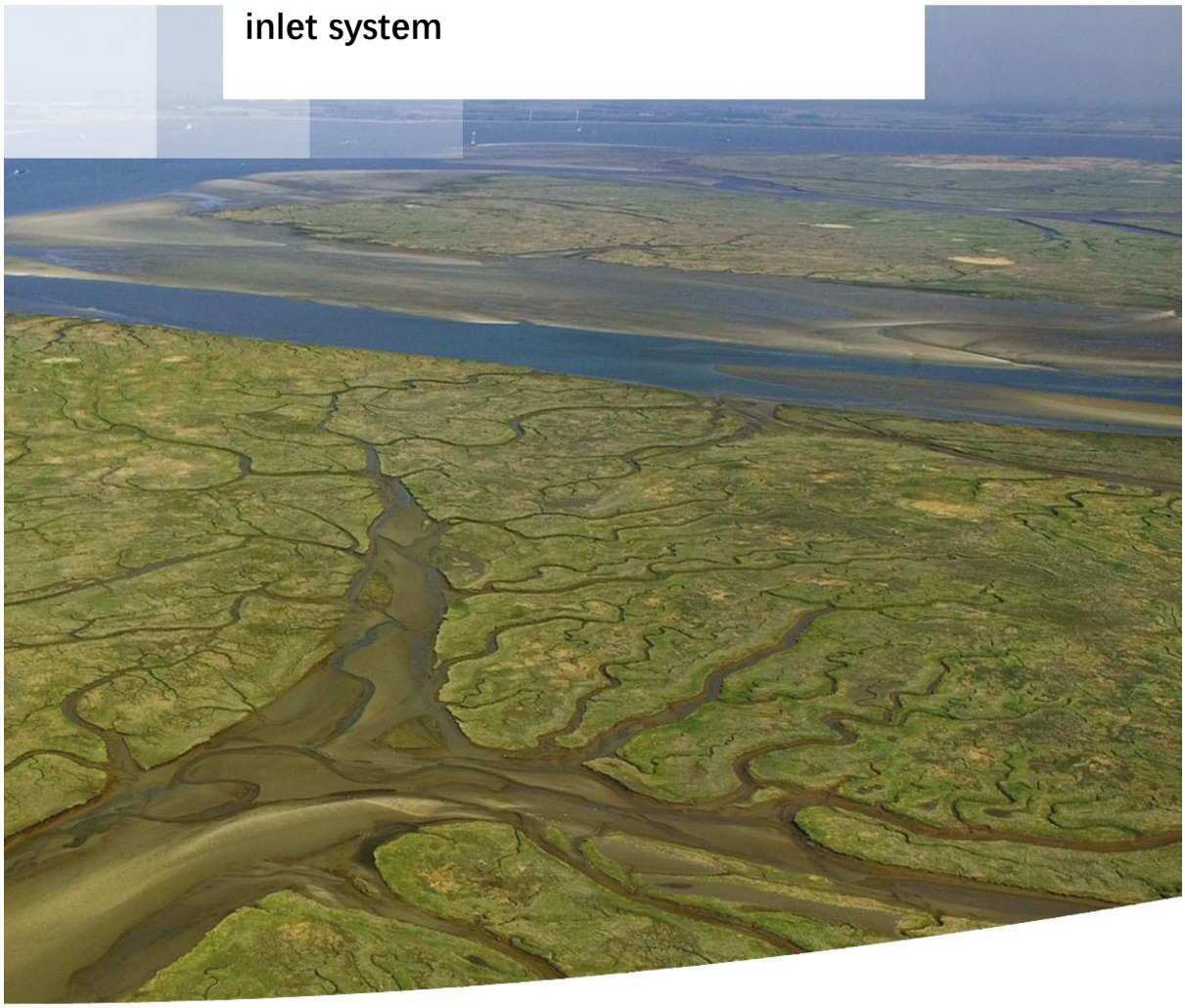

The effect of erosion-resistant layers in the subsurface on the morphological evolution of the schematized Ameland inlet system

ShengZhuo Xu

Helena van der Vegt

Marc Hijma

Maarten van der Vegt

Abstract

Many countries have vital concerns on their coastal safety because about 40 % of the human population is located within 100 km of the coast. Therefore, it is important to understand how the coast will evolve in the future. As one of the most important coastal features of the Dutch coast, the tidal inlet system has drawn a lot of attention from many researchers. The prediction on long-term evolution of tidal inlet system has been studied by the means of numerical modeling. However, lots of models did not include the influence of erosion-resistant layers, which is one of the determining factors of the morphology in a tidal inlet system. The aim of this study is to induce the erosion-resistant layer to the subsurface of the model and investigate the influence of depth, erodibility and adding erosion-resistant patches on the evolution of tidal inlet morphology. Therefore, a process-based model was built in this study based on the model proposed by Dissanayake et al. (2009) for a schematized Ameland inlet and was simulated with Delft3D. An erosion-resistant layer was incorporated by setting the critical shear stress for erosion of the cohesive sediment fraction to an extreme value so that it became hardly erodible. In order to look at the effect of depth, erodibility and spatial adding erosion-resistant patches respectively, three groups of simulations were defined. Variations within each group was investigated by analyzing overall morphology, channel geometry and sediment budget. The result suggests the depth, erodibility and adding erosion-resistant patches have significant but also diverse influence on morphology, channel geometry and sediment budget of the system. The common influence observed in all scenarios are (1) erosion-resistant layers are able to hinter the main channel from incision of the subsurface; (2) erosion-resistant layers can lead to more erosion on the eastern barrier islands. The rest of the effects varies depends on the model setting. The writer assumes that these behaviors can be attributed to the change in flow velocity. The result from this study was later compared with other researches on erosion-resistant layers. Besides, the study has some limitation as well, which is induced by grid resolution, simulation period and lack of lateral erosion.

For future studies, the recommendations are (1) to have a finer grid system to improve the accuracy so that the model can be used to investigate the migration of tidal channels; (2) to extend the simulation period till all the simulation reached its (dynamic) equilibrium state; (3) to shrink the domain area for the sack of computational speed. In addition, the future study should implement more quantitative analysis in order to describe the result in a more reasonable way. (4) there should be more quantitative analysis for model result interpretation.

Contents

Introduction

This report was carried out for Deltares within the framework of 'KPP B&O kust' program of Rijkswaterstaat with the overarching goal to improve the predictive power of hydromorphological models by incorporating geological information. The study was supervised by Maarten van der Vegt (University of Utrecht), Marc Hijma (Deltares) and Helena van der Vegt (Deltares).

1.1 Background

In the Netherlands, and many other countries, it is crucial to predict the evolution of the coast line over the next decades or centuries with reasonable certainty (Hijma, 2017b), since it impacts maintenance of existing coastal infrastructures, flood-defense plans and future management of the coastal area. One of the major coastal features in the Netherlands are the tidal inlet-barrier systems, which locate between the Friesland and Groningen provinces and the North Sea. Tidal channels typically migrate and erode through various sediment bodies with diverse grain sizes, shell content, mud percentage and other sediment properties (Hijma, 2017b). Thereby, tidal inlet morphology is to some extent determined by the spatial distribution of sediment properties in the shallow subsurface. Many of the predictions of tidal inlet evolution and tidal channel migration use numerical models such as Delft3D (e.g. Dissanayake et al., 2009; Dissanayake et al., 2012; Elias & Hansen, 2013; Lenstra et al., 2019). However, most of these existing models do not consider subsurface stratigraphy in the model parameterization.

The report of Hijma (2017b) includes a qualitative description, based on quantitative data, of two scenarios of how migration rates and channel morphology are affected when erosion-resistant layers are present (Figure 1). Panel A represents the case that channel can migrate freely through loose sand bodies to the east, creating a smooth profile line on the side of the channel. After a certain period (Panel B), the channel encounters the erosion-resistant deposit on the east side so that a staircase-profile is formed, and the migration speed decelerates. Since hindered on the side, the channel will start to erode more deeply. Panel C illustrates another scenario where erosion-resistant layer is located at the bottom of the channel. In this case, the channel is rendered shallower and wider. In order to quantitively study the influence of erosion-resistant deposits on tidal channels, Hijma (2017b) used contour-line (the lines of -6 and -15 meters) migration and reconstructed thalwegs (Cleveringa and Geleynse, 2017) in ArcGIS to plot the channel migration speed map and further compare that with the geological content map. However, the relationship between erosion-resistant deposit and migration speed is not proven since there are also many other factors influencing the migration speed.

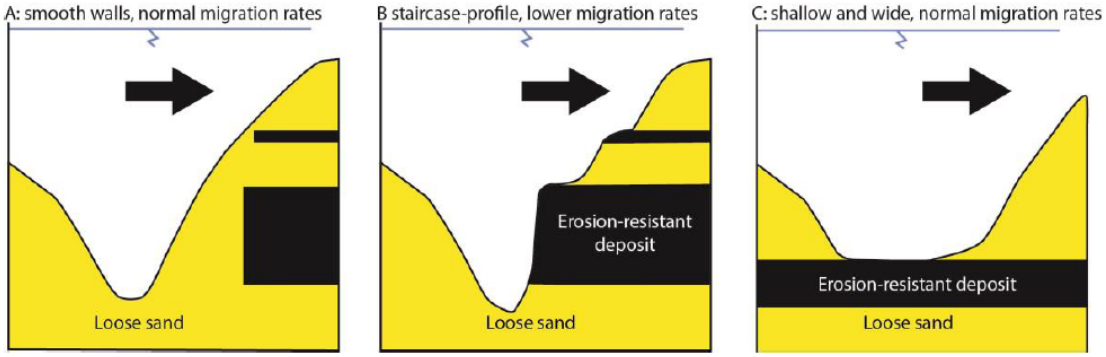

Figure 1. The schematic plot of the effect of erosion resistant deposit on the migration of tidal channels (Hijma, 2017).

1.2 Study area

The Ameland Inlet is the least artificial inlet system within the Dutch Wadden Sea (Elias et al., 2012) and has minimal connectivity to adjacent basins during the calm weather, thereby it can reasonably be schematized as an isolated basin (Ridderinkhof, 1988; Cheung et al., 2007; Dissanayake et al., 2012).

The local tidal amplitude is around 2 meters, propagating from west to east (Dissanayake et al., 2009); the average significant wave height is 1.1 meters coming from northwest and the tidal prism is 480 million m^3 (Sha, 1989). Eastward-oriented tidal channels are present inside the basin (Dissanayake et al., 2009), as shown in Figure 2. Ameland inlet, as other inlet system in the Dutch Wadden Sea, has a clear cyclic evolution (Israel and Dunsbergen, 1999), which means that the sandy shoals will migrate from the updrift to the down drift repeatedly and the orientation of the channel swings between northwest and northeast. According to the estimation of Ridderinkhof et al. (2016), the period of this behavior is 60 years.

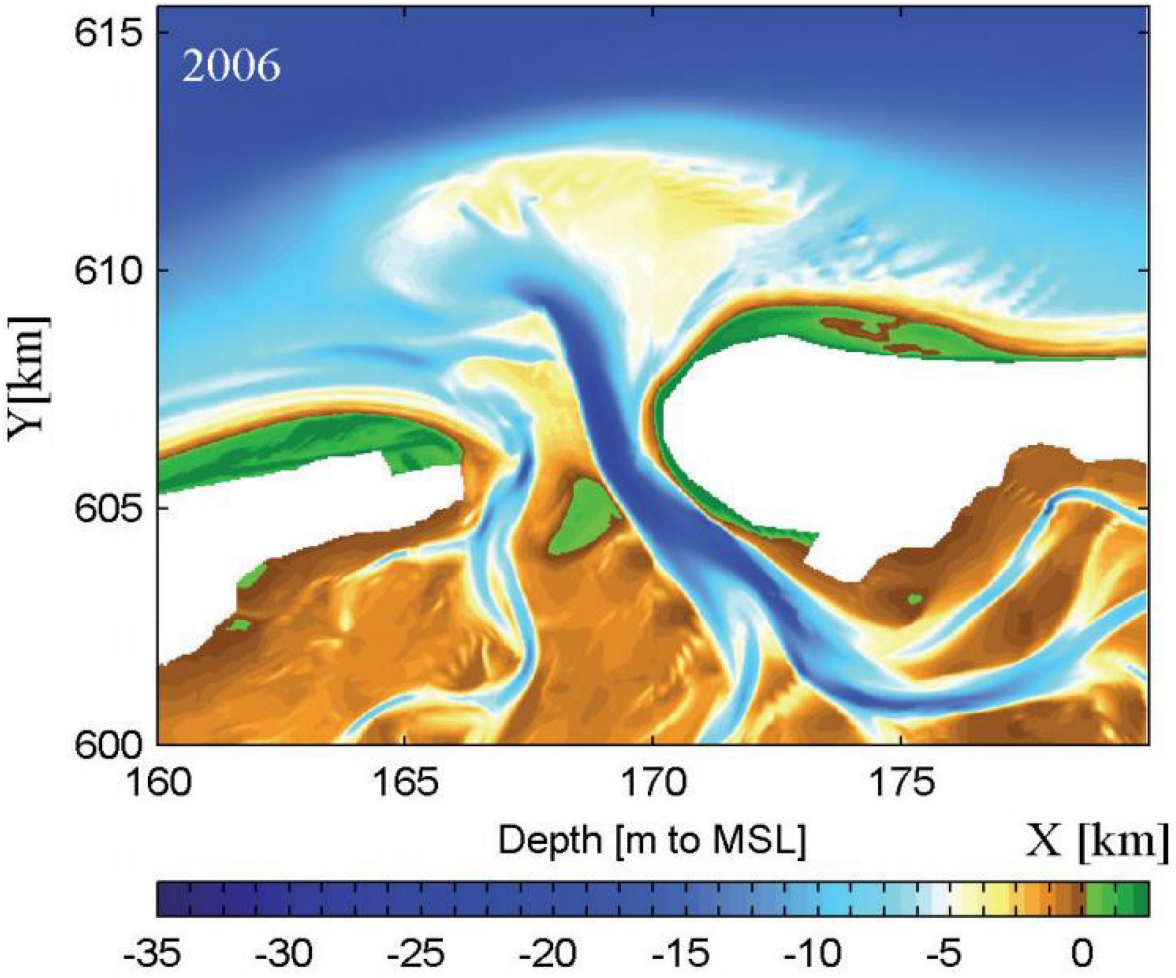

Figure 2. The topography of Ameland inlet system in 2006 (Elias et al.., 2012)

According to Sassi et al. (2015), the Ameland inlet and associated the ebb tidal delta mainly consist of sediment with a diameter of 250 μm (d50) while the grain size is much finer inside the basin, around 100 μm (See Figure 3).

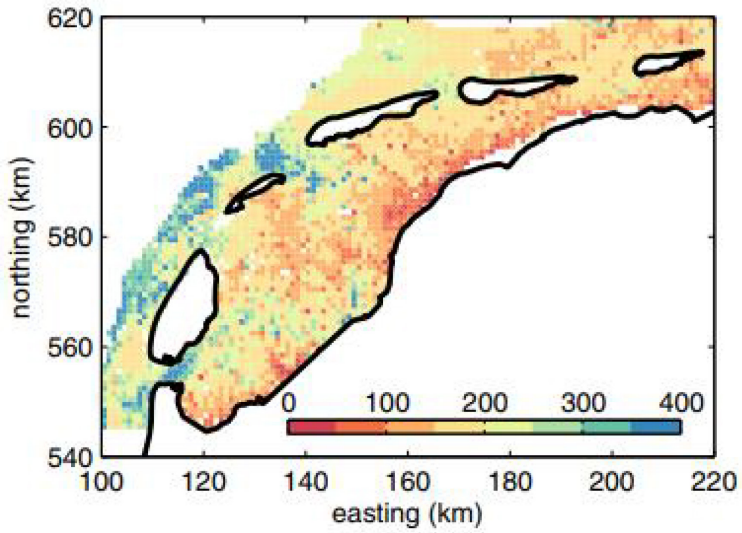

Figure 3. Spatial distribution of sediment grain size in part of the Dutch Wadden Sea (Sassi et al., 2015).

In Ameland region, there is a difference in stratigraphic build-up between the inlet area and the tidal basin area. The subsurface of the inlet area consists of around 20 meters of predominantly sand relative to mean sea level (Figure 4). Underneath the sand, from a depth of approximately 23 meters below mean sea level, lies a layer of Plotclay (Van der Spek, 1994; Hijma 2017a). Therefore, there is deep incision and sediment reworking in this region, e.g. the main channel of the tidal inlet can reach depths of up to -23 meters. The Potclay layer may therefore become exposed to the flow in places, which hinders the channel's ability to erode further into the subsurface. On the other hand, the tidal basin area has older Pleistocene sediment and they have hardly been reworded. Salt marsh deposits can be found on the landward side of the barrier islands and on the coast of the mainland. The sediment composition mainly consists of sandy deposits near the inlet while almost clayey at the landward boundary (Van der Spek, 1996), which is caused by landward accumulation of suspended sediment and the decay in tidal force (Postma, 1954, 1961; Van Straaten & Kuenen, 1957; De Glopper, 1967).

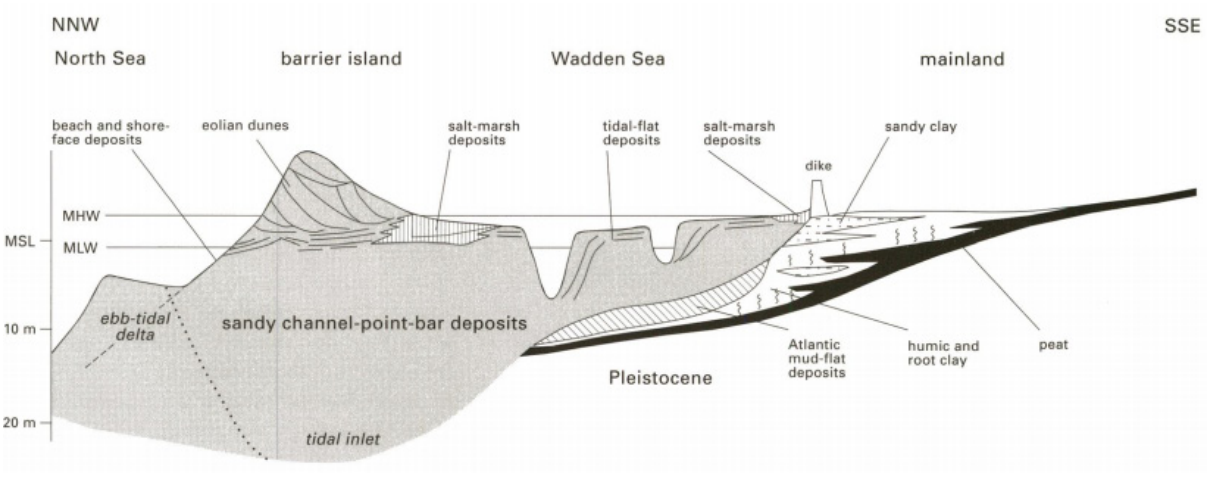

Figure 4. Hypothetical cross-section through the central part of the Dutch Wadden Sea and the Frisian mainland (Van der Spek, 1996).

The monitored channel depth profile of the Ameland inlet is shown in Figure 5 (Forzoni et al., 2018). After the observation of the stair-wise profile, the researcher took several samples. They found a Holocene clay layer at -13 meters and a Potclay layer at -23 meters.

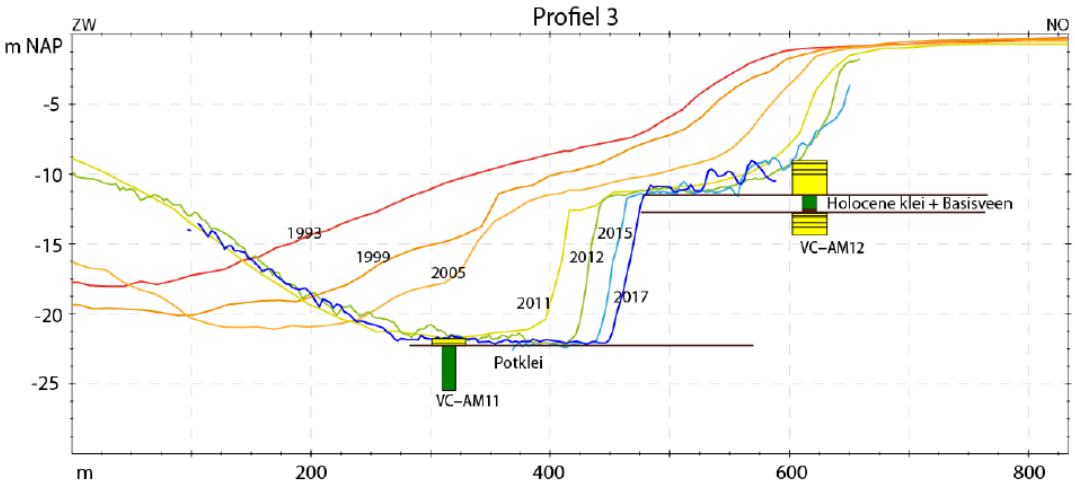

Figure 5. The development of channel section of the Ameland inlet between 1993 and 2017 and the presence of clay layers (Forzoni et al., 2018)

Migration of tidal channels and tidal inlets in the Ameland inlet region has reworked the Holocene deposits (Van der Spek, 1996). In the period between 1831 and 1984, 47% of the surface area was reworked by migrating channels deeper than 2.5 meters (Figure 6). The total reworked sediment volume reached 670 million m^3, which is 4.4 million m^3 annually.

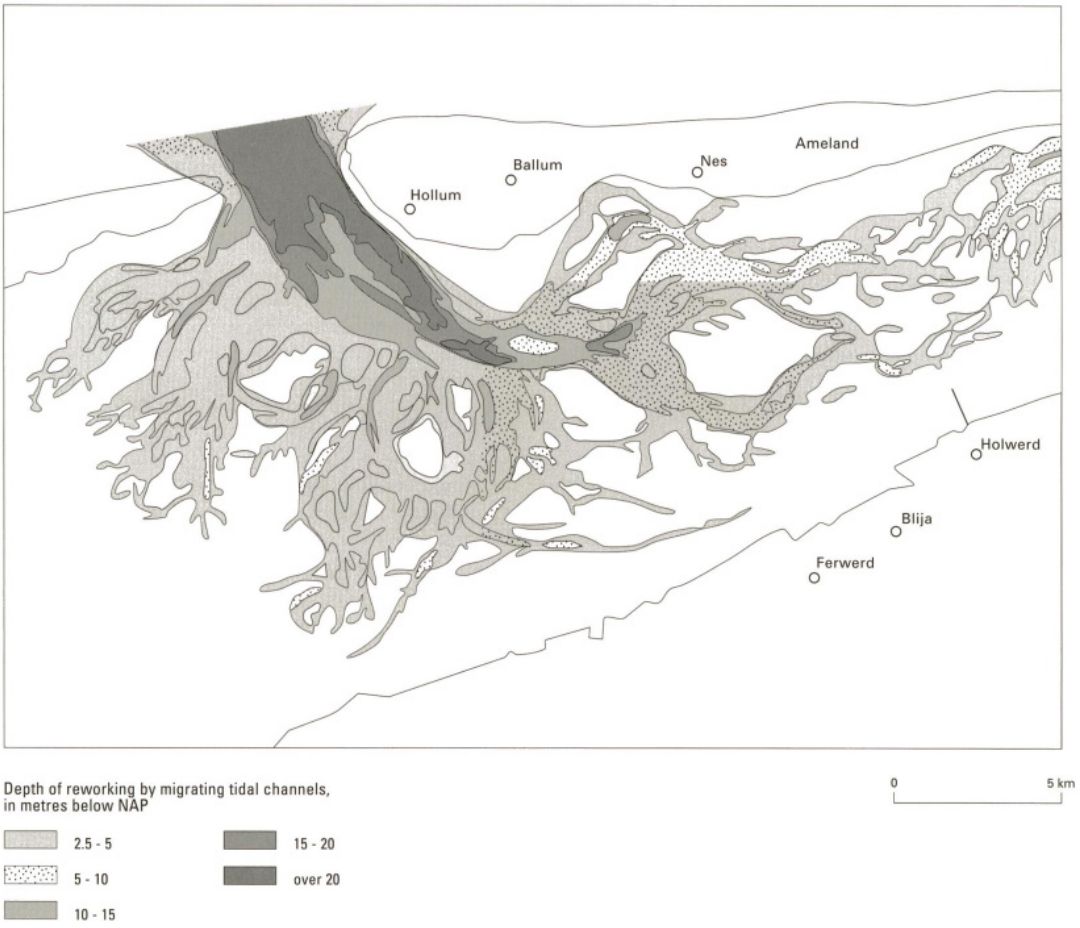

Figure 6. Map of depth and areal extent of sediment reworking by migrating tidal channels deeper than NAP -2.5 meters in the Ameland inlet region between 1831 and 1984 (Van der Spek, 1996).

1.3 Research question

The objective of this study is to investigate the effect of erosion-resistant deposits on tidal inlet morphology. The research questions to be answered in this study are:

1. Does the erosion-resistant layer in the subsurface affects the morphology of the tidal inlet? If so, how does the morphology differ with different depth of the erosion-resistant layers?

   To address this question, a schematized Ameland Inlet model was built based on the model of Dissanayake et al (2009). In order to examine the effect of an erosion-resistant layer in the subsurface, one simulation without this layer was carried out and the results were compared with the scenarios with erosion-resistant layers at different depths.

2. What is the effect of the erodibility of the erosion-resistant layer on the morphology of the tidal inlet?

   In real cases, erosion-resistant deposits have various erodibility, which might affect the deepening and lateral migration of the channel if they are located underneath the channels. The critical shear stresses for erosion of erosion-resistant deposits have not been studied in the field yet. In this study, we assigned five idealized erosion critical shear stresses ranging from 4 to 20.

3. What is the influence of adding shallower erosion-resistant patches on tidal channel morphology?

   In the region of Ameland inlet, there are several patches of erosion-resistant deposits, as shown in Figure 5, which can also be another factor influencing the tidal channel patterns inside the tidal basin. This study included a uniform erosion-resistant layer at -20 meters in depth and a rectangular patch of erosion-resistant deposit at -15 meter on the east side of the channel (See section 2.1 for detailed information).

Methodology

2.1 Modeling system

2.1.1 General description

The model used in this study is based on the model proposed by Dissanayake et al. (2009), which was set up in Delft3D-FLOW/SWAN. Delft3D solves depth-averaged shallow-water equations (Lesser et al., 2004) and wave action balance equations (Booij et al., 1999; Ris et al., 1999; Holthuijsen, 2010). The sediment transport calculations for sand used the formulation from Van Rijn (2004) for non-cohesive sediment, which partitions the transported sediment into bedload and suspended load. The Partheniades-Krone (Partheniades, 1965) formulations were used for cohesive sediment which is assumed to only be transported in suspension. For each calculation time interval, the sediment fluxes between the bed and the water column is determined. Based on this flux, the morphology is updated and then used as the new bathymetry input for the hydrodynamic and sediment dynamic calculation in the next time step. The morphological time scale factor is implemented in order to accelerate the simulation, since the time scale of a morphological development is longer than typical flow changes (Roelvink, 2006). To be more specific, the calculated amount of transported sediment from the sediment module will then be multiplied by this factor, which is the amount of transported sediment in morphological time. Thereby, the value can be used to calculate the bed change in the morphological module. The model calculation is demonstrated as a flow diagram in Figure 7. We implemented a bookkeeping underlayer as well as three sediment fractions, including two non-cohesive sediment and one cohesive (mud) sediment. The cohesive sediment was set to have extreme high erosion critical shear stress, which functioning approximately as erosion-resistant layer located in the subsurface in the reality. The detailed information on sediment module can be found in section 2.1.4.

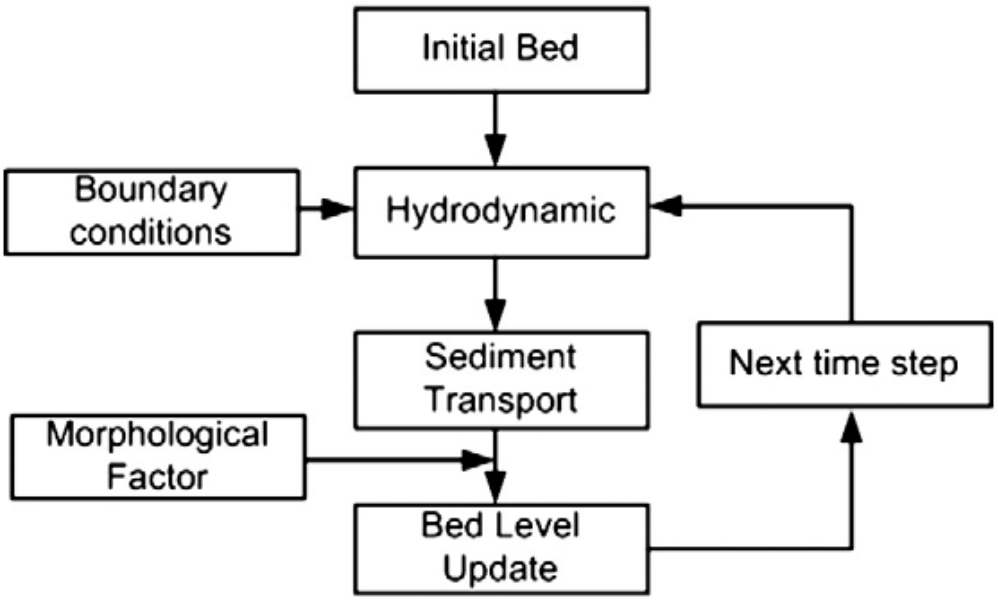

Figure 7. The schematized flow chart of the process-based model (Dissanayake et al., 2009).

2.1.2 Model domain

The model domain in this study is based on Dissanayake et al. (2009). Since the aim of the study is to investigate the influence of an erosion-resistant layer, applying a schematized rectangular tidal basin, channel and sea region can allow us to neglect several factors (e.g. the uneven bathymetry, irregular shape of the land boundary and sophisticated hydrodynamic conditions) and focus on morphological evolution (Dissanayake et al., 2009). As shown in Figure 8a, the dimension of the open sea area is 60

km in width and 24 km in length. The inlet channel is located in the middle of the southward boundary of the open sea area, with a width of 3 km and a length of 3 km. The connection between the inlet region and the tidal basin is located at the western part of the tidal basin in order to approximate the morphology of Ameland Inlet. The tidal basin is 24 km in width and 13 km in length. We also implemented a schematized bathymetry to the system, as shown in Figure 8b. The depth of the channel and the tidal basin is 3 meters. Then, the depth gradually decreases from 3 meters to 20 meters from 16 km to 25 km (distance from the see boundary). The remainder of the open sea area has a uniform depth of 20 meters. The grid system is not equidistant in vertical and horizontal direction to maintain both the acceptable computational speed and desirable accuracy in the interested area. Grid size varied from 2000m×1800m at the two endpoints of north boundary to 200m×150m in the inlet channel (Figure 8c).

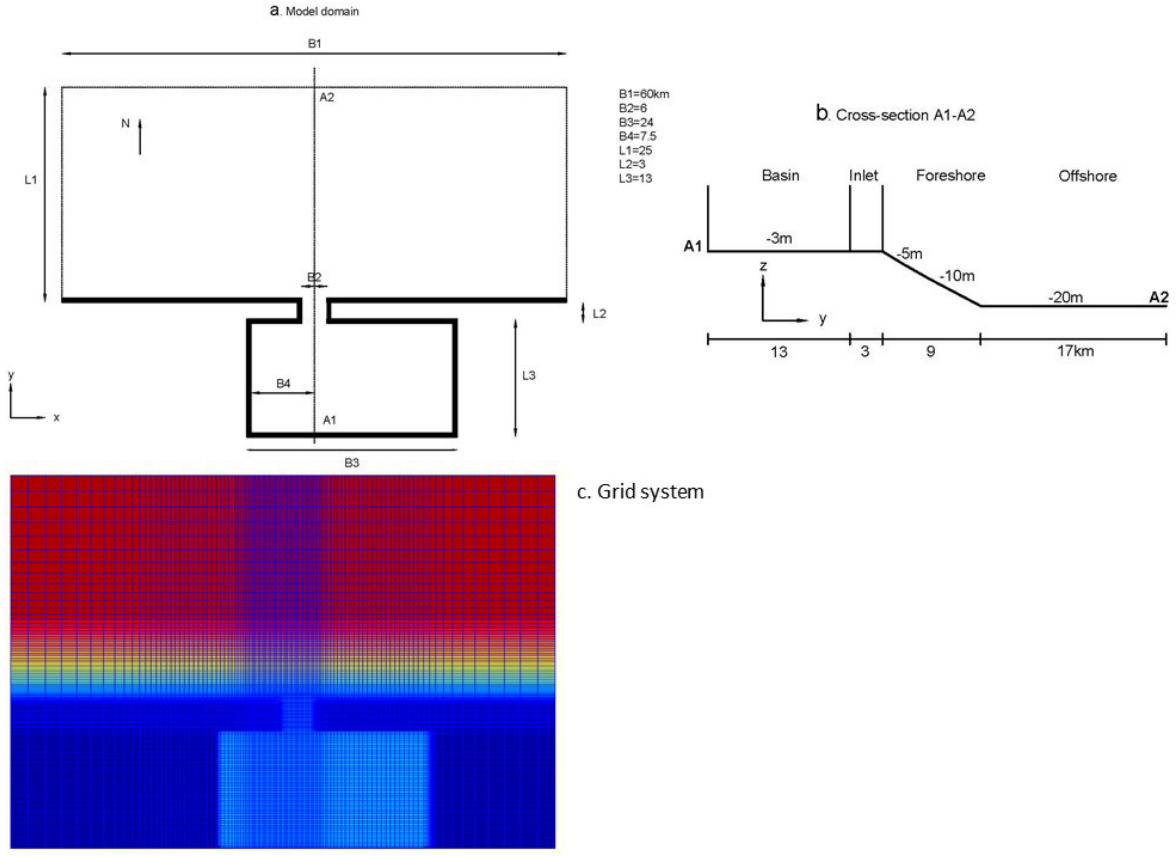

Figure 8. (a) The dimension of the model domain; (b) the profile of cross-section A1-A2; (c) The grid system of the model.

2.1.3 Hydrodynamics

The hydrodynamic condition from Dissanayake et al. (2009) were used, which was derived from a well calibrated 2DH model covering the North Sea (Roelvink et al., 2001). In Delft3D-FLOW, the hydrodynamic timestep is 0.5 minutes. The northern boundary is represented by 3 astronomy tidal constituents, namely M2, M4 and M6. Neumann boundary conditions were assigned to the lateral boundaries which simulates the alongshore water gradient. A wave module in Delft3D-SWAN was online coupled to Delft3D-FLOW every 60 hydrodynamic minutes (120 computational timesteps). The significant wave height was set to 1.4 meter and wave period was 7 seconds. Waves comes into the system from the northern boundary with a clockwise 330-degree angle referring to the north axis (Dissanayake et al., 2009).

2.1.4 Sediment transport

There are in total three sediment fractions in the sediment module, including two non-cohesive sediment (sand) and one cohesive sediment (mud). The original model from Dissanayake et al. (2009) implemented a single sand fraction. However, in order to make the result more comparable to Ameland inlet system, two non-cohesive sand fractions were included in the sediment module, with D50 equaling 250 μm and 100 μm respectively. Furthermore, cohesive sediment was used to approximate erosion-resistant deposit by assigning an extremely high critical shear stress value to this sediment type. However, it became clear that this parameterization could lead to unwanted side-effects in Delft3D. When the cohesive sediment is eroded and then re-deposited elsewhere, the sediment parameters (e.g. critical shear stress for erosion) remains unchanged. Consequently, various regions of the domain can be covered with a newly deposited layer of erosion-resistant sediment, which does not approximate real-world behavior. In contrast, when sediment is eroded from the hard layer in a natural system and deposited elsewhere, it is more likely to have a much lower critical shear stress for erosion after re-deposition. This problem is addressed by switching off the deposition process of the cohesive sediment using the 'Depeff' keyword in Delft3D.

Selection of the transport formula

There are three commonly used transport formulas, namely Van Rijn (1993), Van Rijn (2007) and Engelund-Hansen (1967). Engelund-Hansen (1967) was excluded from the sensitivity test since it does not allow for wave-driven sand transport. The sensitivity test results suggested that Van Rijn (2007) produced better channel patterns. See Appendix for more information.

Selection of the representative diameter of suspended sediment

The representative diameter of suspended sediment $D_s^{(\ell)}$ is by default calculated by medium sediment diameter multiplied by the user-defined factor (1 as default). When 'Iopsus' is set to 1, it can be replaced by another way of calculation which is based on the non-dimensional bed shear stress. Please refer to Delft3D manual (Deltares, 2018) for more detailed information. Both methods of determining the representative diameter of suspended sediment were tested. The comparison of the results showed that Iopsus = 1 generated more realistic channel patterns.

2.1.5 Morphodynamics

To implement erosion-resistant deposits at a specified depth, a bookkeeping underlayer system (Van Kessel et al., 2012) was implemented with 80 layers of 0.5 m thickness. Subsequently, an initial bed composition file was used to specify the initial composition of multiple layers including depth, thickness and fractions of each sediment type. In this study, the original model was set to have an erosion-resistant layer at -20 meter in depth for the whole domain. Note that this depth is defined as 20 m below the initial depth of the channel of 3 m below mean sea level, meaning that the erosion-resistant layer lies at 23 m below MSL/NAP and plots at -23 m in the figures. The sand layers above and underneath the hard layer consist of 50% sand with 250 μm and 50% sand with 100 μm. The depth of the erosion-resistant layer was varied later to study the effect of depth on tidal channel pattern formation.

Selection of morphological time scale factor (MORFAC)

The selection of morphological time scale factor can be crucial in balancing computational speed and result accuracy. The model started from a relatively homogeneous bed compared to the natural morphylogy of the Ameland inlet. This situation could lead to significant bed changes in the beginning of the simulation. These changes can result in irreversible patterns when using a too large morphological time scale factor (Dissanayake et al., 2009). The best way to determine the most appropriate morphological factor is to do several test runs and choose the largest value whose result does not significantly differ from the results of the simulation with the smallest value. The sensitivity tests

included MORFAC values of 25, 30, 40 and 50, 25 as the smallest value due to calculation time considerations. The result showed that 40 is the most appropriate value for morphological time scale factor.

Selection of dry cell erosion factor (ThetSD)

The aim of the study is to focus on the evolution of tidal inlet morphology, eroding the dry banks on the sides of the inlet, where local bathymetry is above the water level. The default setting of Delft3D erosion can only take places where there is flow velocity and water depth, even when an overly steep bank is created to the adjacent dry cells (Deltares, 2018), as shown in Figure 9. This behavior can be improved by a parametrized redistribution of erosion quantity to the surrounding areas. The erosion of adjacent dry cells is then determined by a dry cell erosion factor (ThetSD) Here we also tested the difference between switching on (ThetSD = 1) and off (ThetSD = 0) the dry cell erosion factor. Result suggested that when this mechanism is present (ThetSD = 1), the channel can migrate freely and gradually.

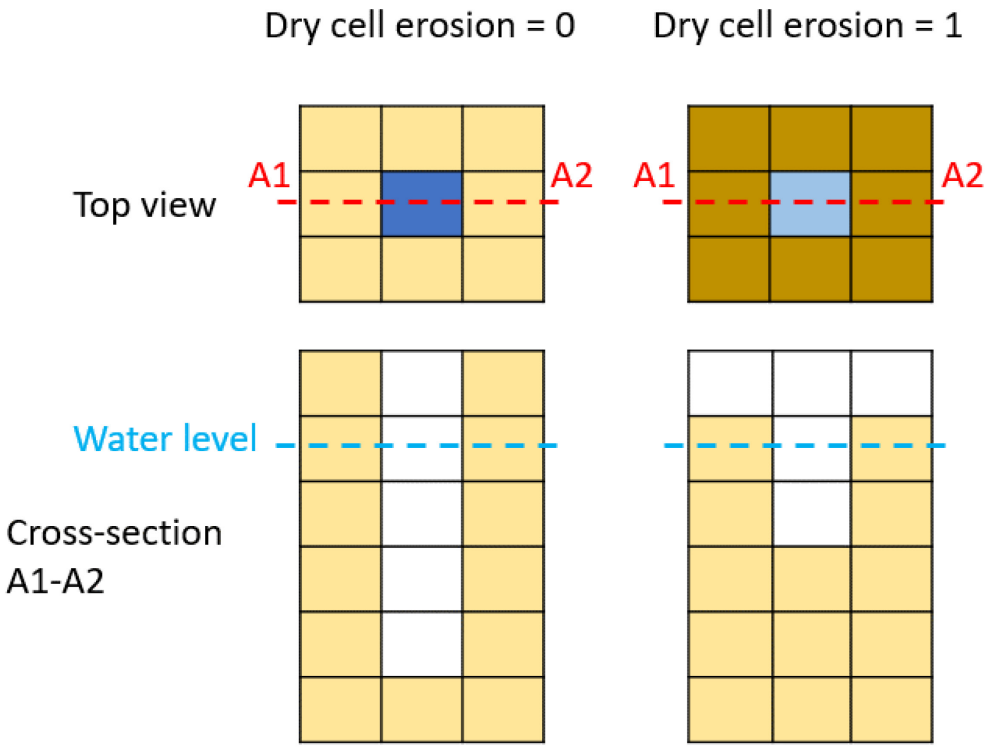

Figure 9. The schematized diagram of the result of different settings for 'dry cell erosion'.

2.2 Scenarios

In order to investigate the effect of depth, erodibility and spatial adding erosion-resistant patches on morphological evolution of the inlet system, three simulation sets were defined (Table 1). The default case was set to have a single spatial uniform erosion-resistant layer at -23 meters NAP with the critical shear stress for erosion equaling 20. The following three groups is based on the default case and only varying the target properties within each group. Note that A_04, B_01 and C_02 are the default case but were assigned different Run ID for clearer illustration.

Table 1. The list of scenarios in this study. A_04, B_01 and C_02 are bold here because these are the default cases.

Group A: to study the effect of presence of erosion-resistant deposit and its depth on tidal inlet morphology	
RUNID	Depth
A_01	No erosion-resistant layer
A_02	Resistant layer at -33 meters NAP
A_03	Resistant layer at -28 meters NAP
A_04	**Resistant layer at -23 meters NAP**
A_05	Resistant layer at -18 meters NAP
A_06	Resistant layer at -13 meters NAP
Group B: to study the effect of different erodibilities on tidal inlet morphology	
RUNID	Tcr.ero (Critical shear stress for erosion)
B_01	**20**
B_02	16
B_03	12
B_04	8
B_05	4
Group C: to study the effect of adding erosion-resistant patches on tidal inlet morphology	
RUNID	Combinations of multiple erosion-resistant layers
C_01	No erosion-resistant layer
C_02	**A uniform erosion-resistant layer at -20 m depth**
C_03	A rectangular patch of erosion-resistant deposit located at the eastern part of the tidal channel at -13 m (See Figure 10)
C_04	The combination of C_02 & C_03 (See Figure 10)

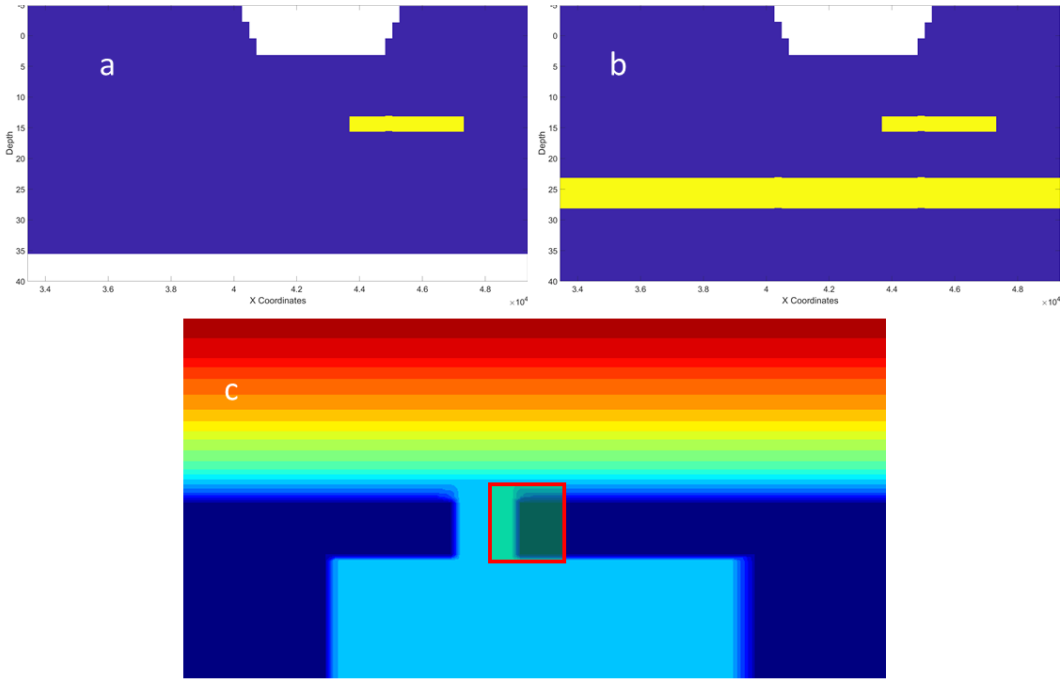

Figure 10. a) The profile view of the channel for C_03. Yellow patches indicate the erosion-resistant layers. b) The profile view of the channel for C_04. Yellow patches indicate the erosion-resistant layers. c) The position of the rectangular patch in C_03 and C_04.

2.3 Data Analysis

Post processing of the simulation results were done in Matlab and investigates three aspects of tidal system evolution: overall morphology, channel geometry and sediment budget. The components in every aspect are also shown here:

The aspect of overall morphology includes the morphology map of simulations after 20 years in order to give a qualitative measure of the differences in inlet morphology between the different scenarios. The main features of a tidal inlets system which are discussed are:

- the ebb tidal delta,
- the inlet, and
- the intertidal channels in the tidal basin.

However, the presented morphologies only represent a snapshot of the morphological evolution. To get a better understanding of the evolution of such a channel, the morphology of different stages of evolution are also presented for the reference model.

Channel geometry considers the evolution of the main tidal channel, which confines the flow and is one of the most dynamic area. It is hypothesized to be the deepest are in the system, experiencing direct influence from the erosion-resistant layers. The result shows the evolution of depth in channel profile located in the cross-section CS-2 (Figure 11).

Since we are focusing on the morphological evolution, sediment budget analyses can provide the information on sediment transport in different cases and how that is influenced by erosion-resistant layers. This includes the analysis on channel and the ebb tidal delta. To calculate the channel sediment budget, two cross-sections were pre-defined in Delft-3D (CS-1 & CS-3) which records the cumulative sediment volume throughput. Then, by subtracting the volume of both sections, the net change of sediment volume in the channel can be achieved. The calculation of the budget of the ebb tidal delta was done in Matlab using the time-series of sediment layer position multiplying the sediment volume fraction of each layer. The area used for this calculation is drawn in Figure 11.

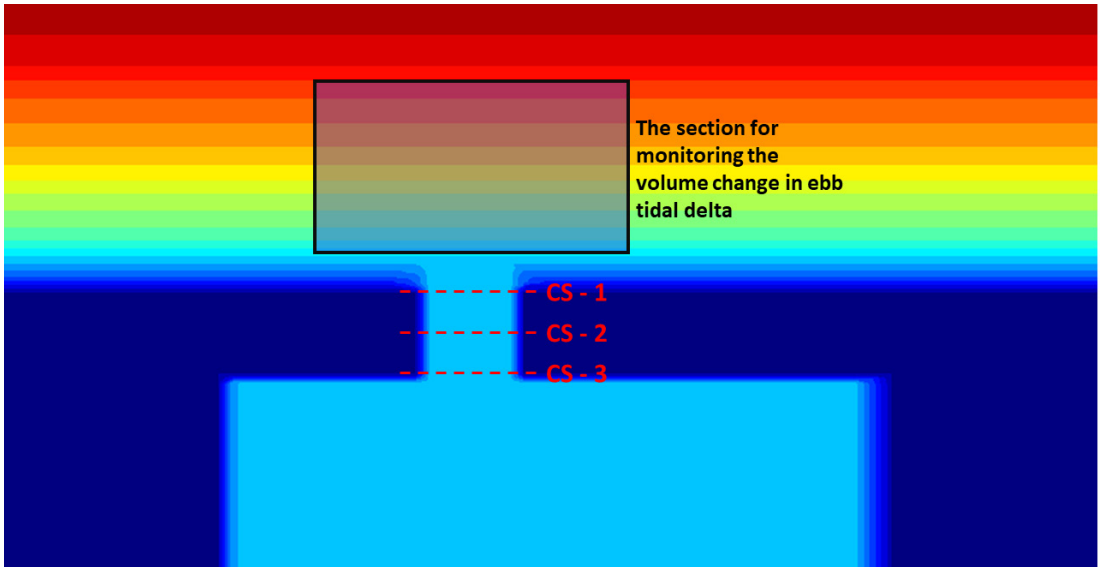

Figure 11. The map of cross-sections and section for data analysis.

Results

The result section consists of 4 parts and each part addresses one topic as followed:

(1) In order to demonstrate the evolution of a schematized tidal inlet with uniform erosion-resistant layer at -23 meters NAP, we present the results of the default simulation, (A_04, equivalent to B_01 & C_02). We let the default simulation run up to 50 years of morphological development so that longer evolution can be observed. The results can also be used to assess whether a dynamic equilibrium state is reached within the 50-year timeframe. We define a dynamic equilibrium as the time when the inlet reaches a steady sediment volume and starts to act as a sediment conduit rather than a sediment source.

(2) Group A Compares the simulation results without erosion-resistant layers to 5 simulation with erosion resistant layers at different depths. addressing research question 1.

(3) Results of group B examines the effect of varying erodibility on tidal inlet morphology, addressing research question 2.

(4) Lastly, the simulations with and without erosion-resistant patches at the channel side will be shown to answer question 3.

3.1 The 50 year-evolution of tidal inlet with erosion-resistant layer

This section presents the result of simulation A_04 (equivalent to B_01 & C_02, Table 1), the default model with a simulation time of 50 years.

3.1.1 Morphology

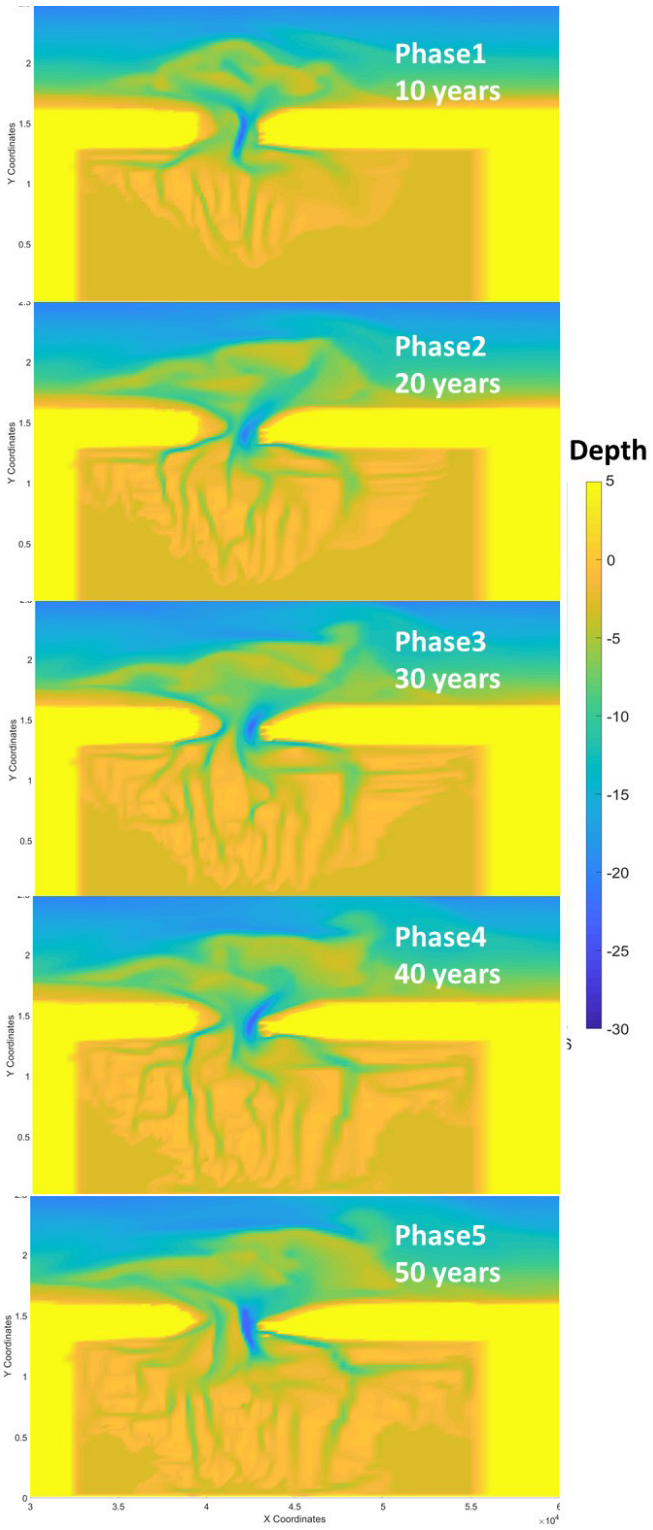

Figure 12. The evolution of tidal inlet up to 50 years with erosion-resistant layer in the subsurface.

Figure 12 illustrates the evolution of the tidal inlet after 10, 20, 30, 40 and 50 years respectively. After 10 years, we can already see that the main tidal channel is narrow and deep, featuring an ebb tidal delta on the seaward side and multiple channels insides the tidal basin on the landward side. After 20 years, the system continues to develop itself. Because comparing with phase 1, the channels in the tidal basin reach further landward and main channel becomes wider. There are two active channels in phase 2.

After that, the overall morphological patterns remain relatively unchanged while the inlet region is still dynamic. However, since these channels have reached the boundary of the simulation by that time it is not possible to say whether this stability is a simply a numerical artefact. The 'cyclic behavior' of the main inlet channel can also be seen in Figure 12. After 10 years, the channel is oriented towards the northwest. Then its orientation shifts towards the northeast and keeps that direction up to 40 years. At last (50 years), the channel starts to move back to northeasterly orientation.

In addition, we can also see that the inlet bounces between a 'one channel system' and a 'two channel system' during the simulation period. When the eastern channel is deep (in 10 years and 50 years), the western channel is negligible in depth. When the eastern channel is shallow (in 20, 30 and 40 years), the western channel is more pronounced and drains the western part of the tidal basin.

3.1.2 Channel profile geometry

The evolution of channel profile at CS-2 is plotted in Figure 13. The channel starts with a flat profile. After 3 years a deep channel is already formed with the deepest point at -23 meters, which coincides with the top of the erosion-resistant layer. Then the channel gradually migrates from the central part of the inlet ($4.1 \times 10^4 < X < 4.2 \times 10^4$) to the eastern part ($X > 4.2 \times 10^4$) of the inlet after 10 years. From 10 years onwards, the main channel remains at approximately the same location in the later 40-years but varies in depth and width. Meanwhile, the middle ($4.1 \times 10^4 < X < 4.2 \times 10^4$) and the western part ($X < 4.1 \times 10^4$) of the inlet is more dynamic, with frequent deposition and erosion cycles. The depth of the western part ranges between -15 meters and 0 meters. Moreover, the erosion of the eastern barrier island is also pronounced and the eastern bank retreats around 1500 meters after 50 years.

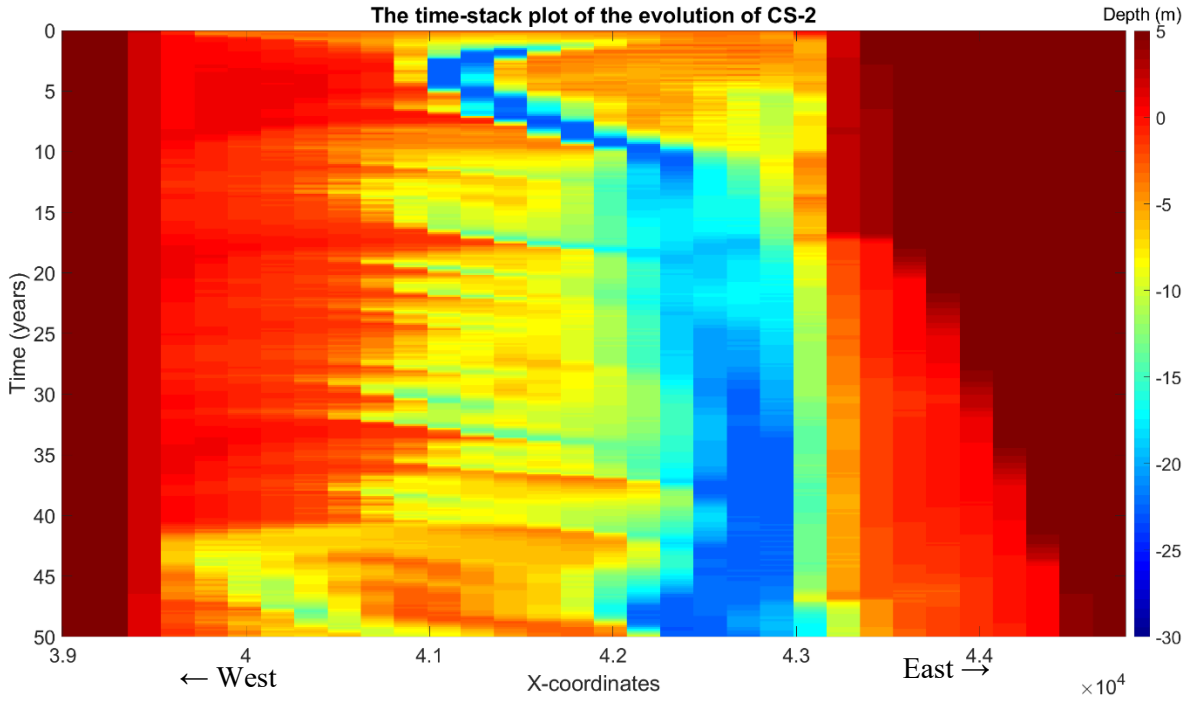

Figure 13. The time stack of depth evolution in CS – 2. The unit of x-axis is in meters.

3.1.3 Sediment budget

The cumulative sediment transport through the northern and the southern boundary is plotted in Figure 14. For both cross-sections, coarse sediment is transported seawards (both red lines > 0) while the transport direction of fine sediment is landwards (both blue lines < 0). The sum of both solid (star) lines indicates there is in total 1.7E+07 (8.5E+07) m^3 sediment transported landwards via CS-1 and CS-3. Furthermore, the inlet region lost 6.8E+07 m^3 sediment after 50 years, within which the coarse sand

fraction was transported to the ebb tidal delta while the fine sand fraction was transported into the tidal basin. The sum of throughput of both sand fractions via both cross-sections reveals the net total sediment volume change of the channel area. In the first 27 years, there is significant sediment loss, around 90 million m^3, in the channel. After that, the channel reached a temporary equilibrium state up until the 45^{th} years. Then the erosion occurs again. After 50 years, there are in total 100 million m^3 sediment lost in the channel. However, the channel region is still functioning as a sediment source so that the system does not reach the equilibrium state yet.

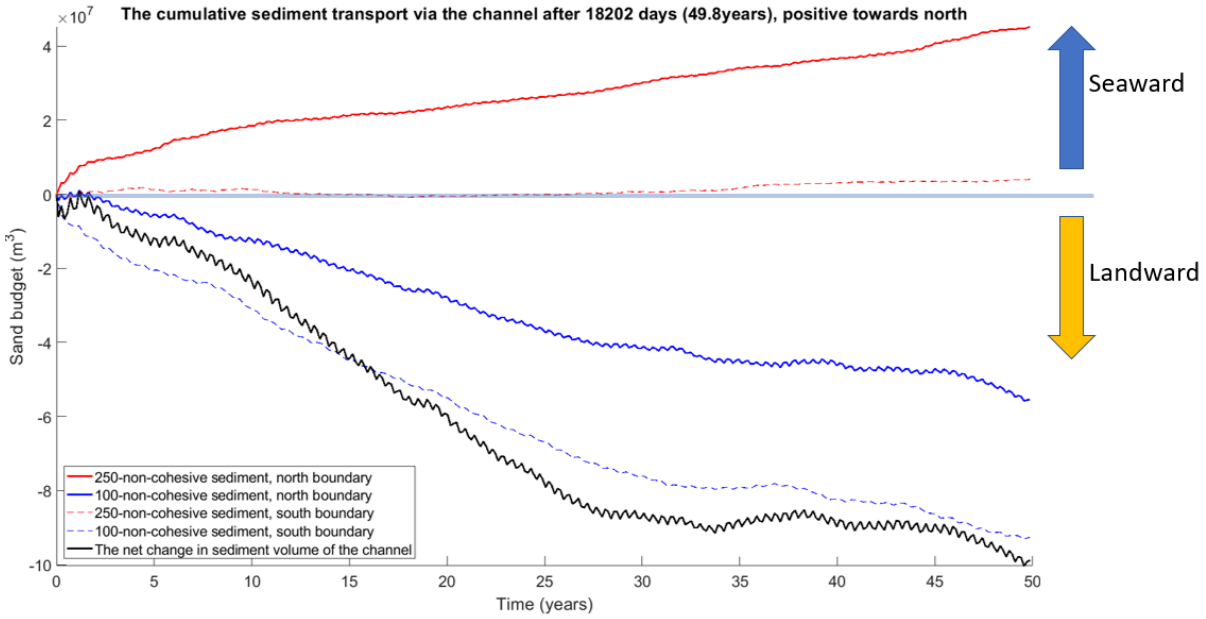

Figure 14. The cumulative sediment transport via CS – 1 (north boundary) and CS – 3 (south boundary) after 50 years.

3.2 Group A: The effect of presence of erosion-resistant layers and their varying depth on the tidal inlet morphology

The scenarios in group A are listed in Table 2.

Table 2. The scenarios in group A.

Group A: to study the effect of presence of erosion-resistant deposit and its depth on tidal inlet morphology	
RUNID	Depth
A_01	No erosion-resistant layer
A_02	Resistant layer at -33 meters NAP
A_03	Resistant layer at -28 meters NAP
A_04	Resistant layer at -23 meters NAP
A_05	Resistant layer at -18 meters NAP
A_06	Resistant layer at -13 meters NAP

3.2.1 Morphology

The morphology map of all six scenarios after 20 years of morphological development is shown in Figure 15. If there is no erosion-resistant layer (A-01), the channel is able to erode to -34.75 meters, which is deeper than the rest of the scenarios. In other scenarios with erosion-resistant layers, the depth of the channels is limited by the depth of the erosion-resistant layers in the subsurface. The width of the inlet (the distance between two barrier islands) is larger in the scenario with shallow erosion-resistant layer. In addition, as the elevation of the erosion-resistant layer increases, the channels in the tidal basin are less well developed.

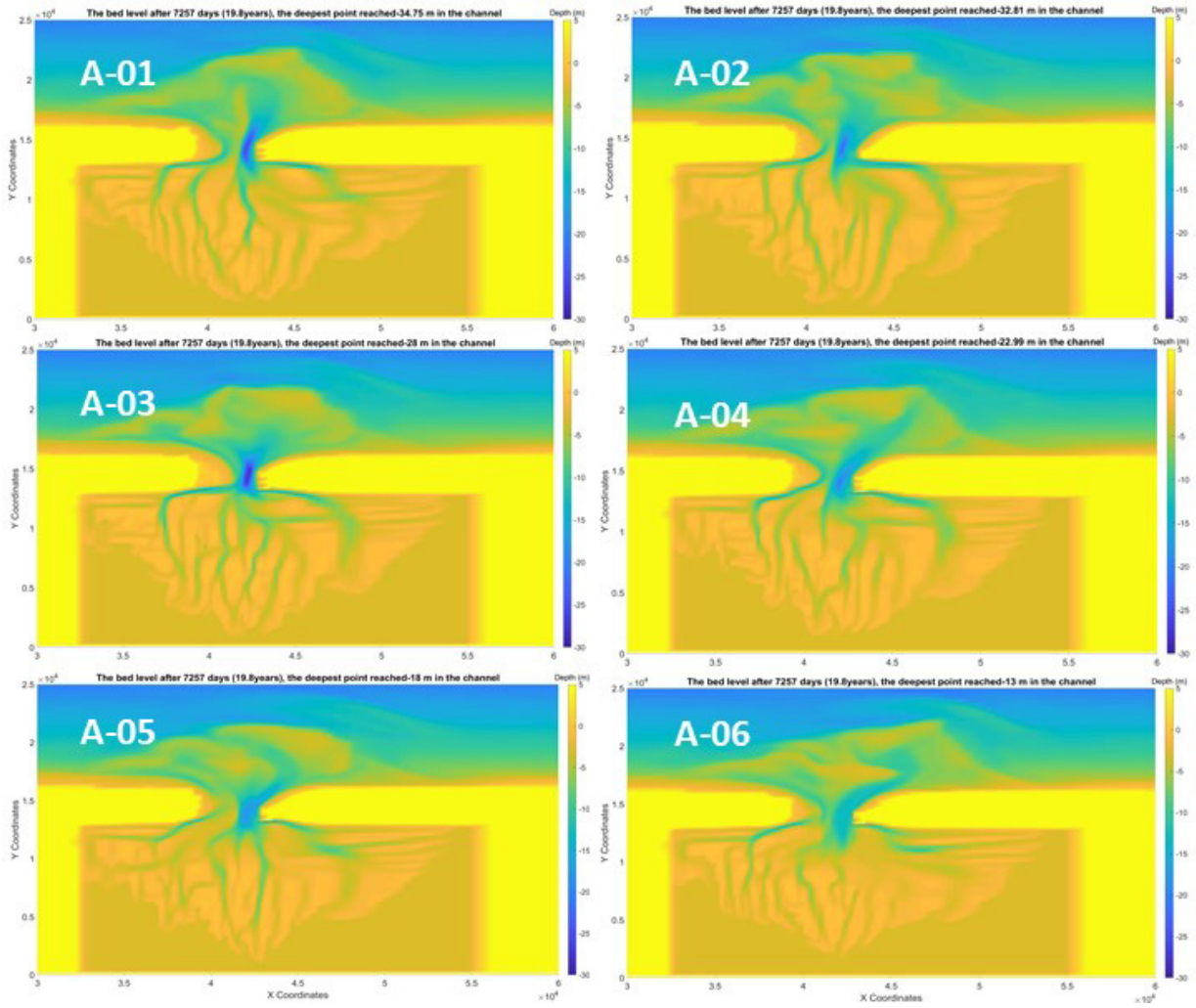

Figure 15.The comparison of morphology map between six scenarios in group A. (1) A_01, no erosion-resistant layer. (2) A_02, erosion-resistant layer at -33 meters. (3) A_03, erosion-resistant layer at -28 meters. (4) A_04, erosion-resistant layer at -23 meters. (5) A_05, erosion-resistant layer at -18 meters. (6) A_06, erosion-resistant layer at -13 meters.

3.2.2 Channel profile geometry

The comparison of time stack plot of depth evolution in group A is shown in Figure 16. By comparing A_01 with the rest of the scenarios, the effect of erosion-resistant layers can be found. The non-erodible layers limit the incision of the channel and prevent the channel from eroding deeper into the subsurface. Furthermore, the area of erosion of the eastern barrier island increases with the erosion-resistant layer becomes shallower, which coincides with the being wider. However, A_02 is an exception here because the erosion-resistant layer is at -33 meters NAP in this scenario while it has the most bank erosion on the eastern barrier island (around 1000 meters in 20 years).

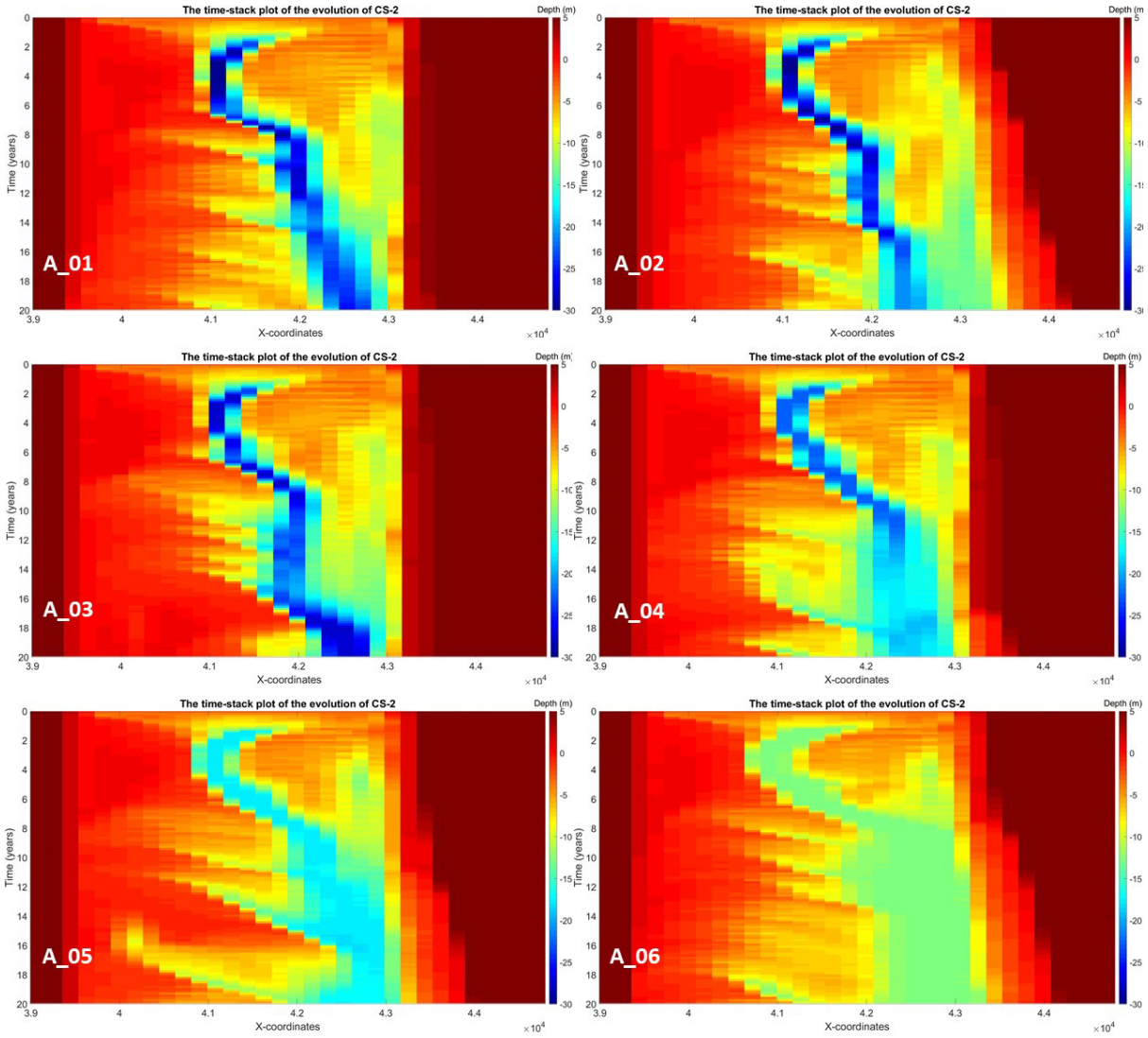

Figure 16. Comparison of time stack of depth evolution of CS-2 in group A.

3.2.3 Sediment budget

The total sediment budget (sum of both sand fractions) of the channel and the ebb-tidal delta was also investigated to better understand of the effect of erosion-resistant layer on sediment transport. Figure 17 presents the sediment budget of the channel for each scenario after 20 years' simulation. In the scenario without erosion-resistant layer (A_01), the channel losses 4.8E+07 m^3 sediment. After adding the erosion-resistant layer into the system, sediment transported via CS-1 shows a decreasing trend as the depth decrease from -33 meters to -13 meters. In the scenario with -18 meters depth, the volume via northern boundary dropped almost 50% compared with the scenario without erosion-resistant layers (A_01). A_03 is an exception here since there is an increase in sediment transport via CS-1 (around 25% of the A_01). The volume change in the sediment transport via CS-2 is also showing a decreasing trend with the increase in depth of erosion-resistant layers, from 6.69E+07 m^3 to 5.85E+07 m^3. By subtracting the volume of sediment entering the channel with the volume leaving the channel, the amount of lost sediment in the channel can be derived. Generally, the presence of erosion-resistant layers can cause slightly more sediment transported out of the system. In other words, more erosion of the channel will occur with the erosion-resistant deposits in the subsurface. However, the effect differs between different depth of erosion-resistant layers.

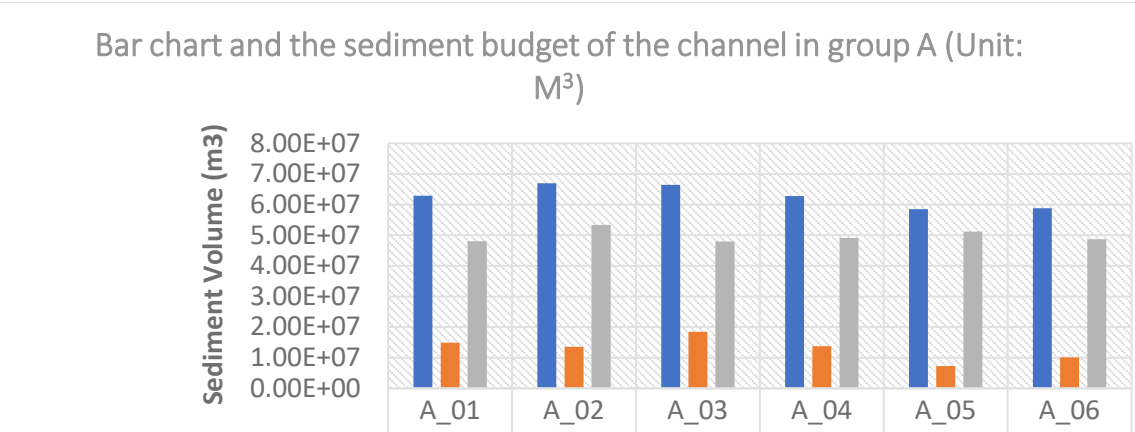

	A_01	A_02	A_03	A_04	A_05	A_06
Transport via CS-3 (positive towards south)	6.29E+07	6.69E+07	6.65E+07	6.28E+07	5.85E+07	5.88E+07
Transport via CS-1 (positive towards south)	1.49E+07	1.35E+07	1.85E+07	1.37E+07	7.30E+06	1.01E+07
Lost sediment of the channel	4.80E+07	5.34E+07	4.80E+07	4.91E+07	5.12E+07	4.87E+07

Figure 17. The bar chart of the sediment budget of the channel in group A, with information on sediment volume attached.

The change in the volume of both non-cohesive sediment type on the ebb tidal delta is plotted in Figure 18. Overall, more coarse sediment (D50 = 250 μm) is transported onto the ebb tidal delta than fine sediment (D50 = 100 μm). When there is no erosion-resistant layer (red line), the ebb tidal delta gains 9E+07 m^3 coarse sediment and 6.5E+07 m^3 fine sediment. Looking at the coarse sediment (solid lines), the deep layers (A_02, A_03) can induce more deposition of coarse sediment while shallow erosion-resistant (A_04, A_05, A_06) layers tend to reduce the deposition of coarse sediment. A_06 is the only scenario where erosion of coarse sediment occurred. All scenarios with erosion-resistant layers start to lose fine sediment after 12 years. The shallower the layers are, the more fine sediment the ebb tidal delta loses.

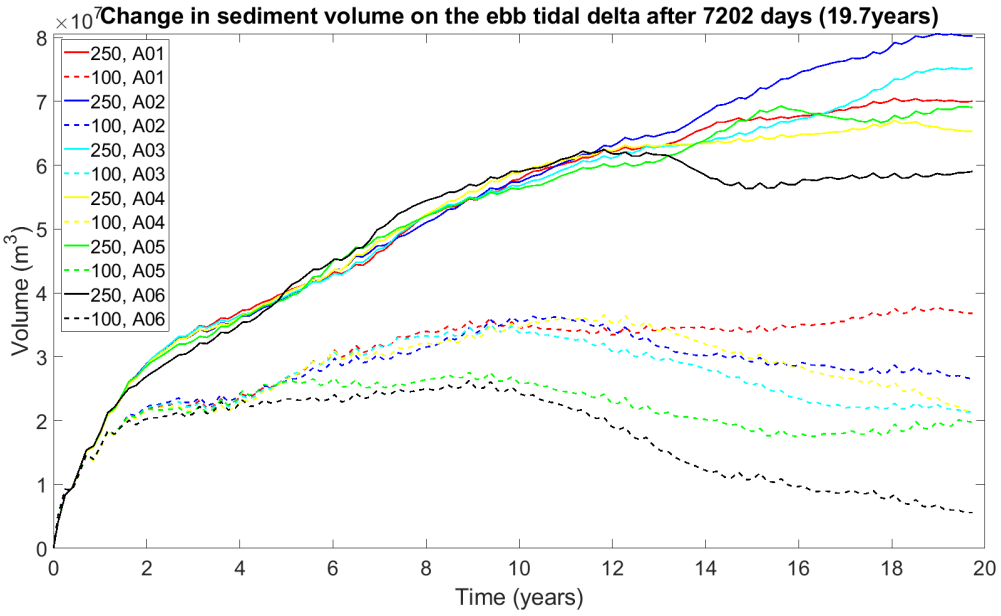

Figure 18. The change in sediment volume on the ebb tidal delta after 20 years simulation (Group A). Solid lines indicate the sediment with D50 = 250 μm and dashed lines indicate the sediment with D50 = 100 μm.

3.3 Group B: The effect of different erodibilities on the tidal inlet morphology

The scenarios in group B are listed in Table 3.

Table 3. The scenarios in group B.

Group B: to study the effect of different erodibilities on tidal inlet morphology	
RUNID	Tcr.ero (Critical shear stress for erosion)
B_01	20
B_02	16
B_03	12
B_04	8
B_05	4

3.3.1 Morphology

The comparison of morphology map after 20 years in group B is shown in Figure 19. The result from B_01, B_02 and B_03 are the same. This indicate that when the critical shear stress for erosion exceeds 12, the erodibilities of the erosion-resistant layers are so similar that they will not lead to visible difference to the morphology of the system. On the other hand, B_04 and B_05 evolved different morphology patterns. The decrease in critical shear stress for erosion (increase in erodibility) of the erosion-resistant layers tends to render the channel deeper and oriented more towards north. In addition, in the scenarios with lower critical shear stress for erosion, the channels in the tidal basin is better developed.

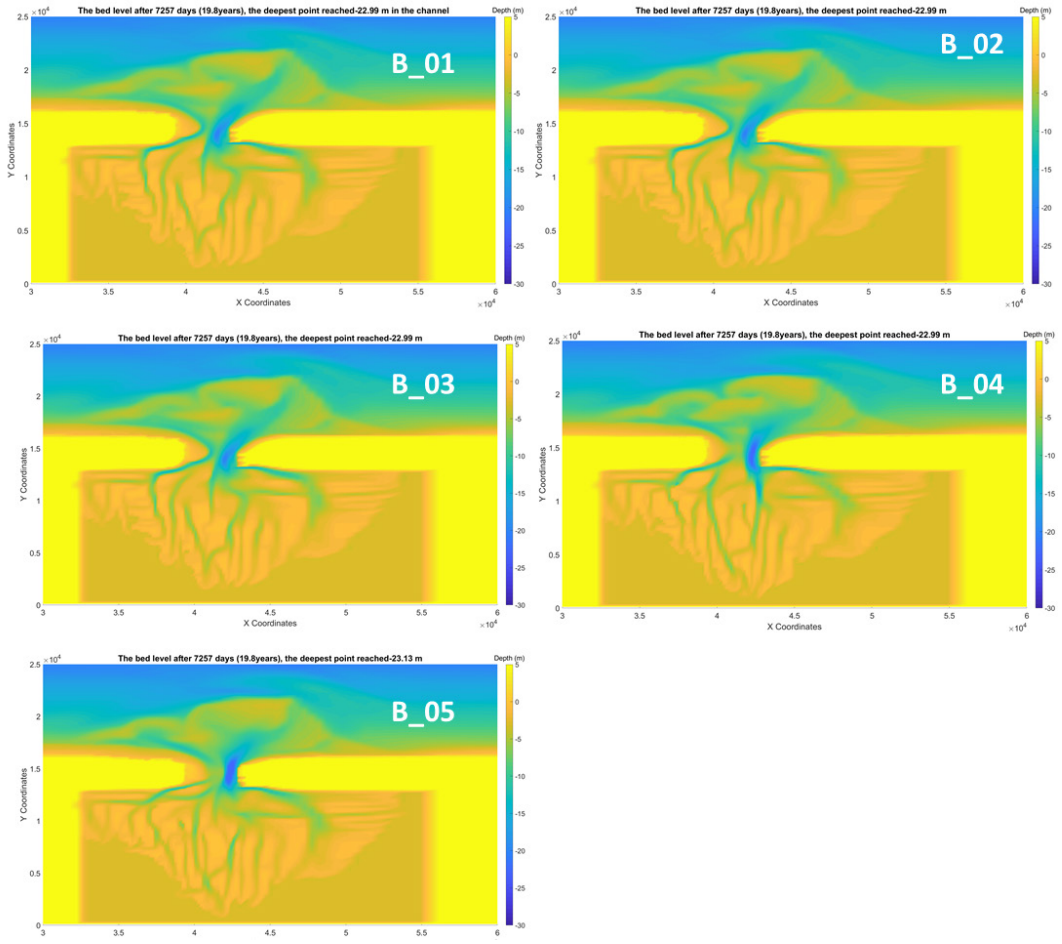

Figure 19. The comparison of morphology maps between six scenarios in group B. (1) B_01 represents the scenario with Tcr.ero = 20; (2) B_02 represents the scenario with Tcr.ero = 16; (3) B_03 represents the scenario

with Tcr.ero = 12; (4) B_04 represents the scenario with Tcr.ero = 8; (5) B_05 represents the scenario with Tcr.ero = 4;

3.3.2 Channel geometry

The comparison of the time stack plot of depth evolution in CS-2 in group B is presented in Figure 20. The result of B_01 & B_02 are left out here and after since they are the same as B_03. For all three scenarios, the depth is limited to be above -23 meters. However, there are more cells reaching -23 meters in B_04 and B_05 than B_03. In other words, the deepest part of the main channel tends to be wider, deeper and more stable at -23 meters as the erodibility of erosion-resistant layer increases.

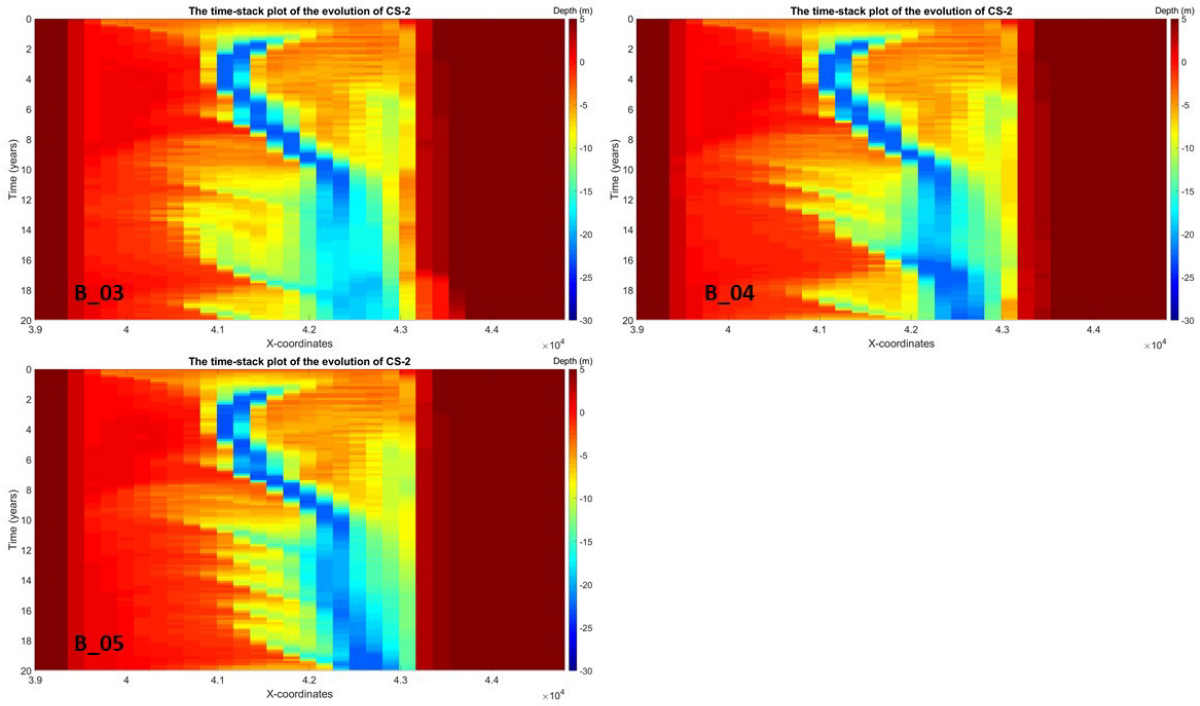

Figure 20. Comparison of time stack plots of depth evolution in CS-2 in Group B.

3.3.3 Sediment budget

Figure 21 presents the bar chart of channel sediment budget in group B, with detailed data attached. The decrease in critical shear stress for erosion (B_03 to B_05) of the erosion-resistant layers leads to decline in amount of lost sandy sediment in the channel, from 4.91E+07 m^3 to 4.09E+07 m^3 respectively. Subsequently, B_03 has the least amount of sediment transported via CS-1 (1.37E+07 m^3) and it increases to 1.93E+07 m^3 in B_04 and B_05. In addition, among the three scenarios, the B_04 has the most sediment transport via CS-2 (6.46E+07 m^3).

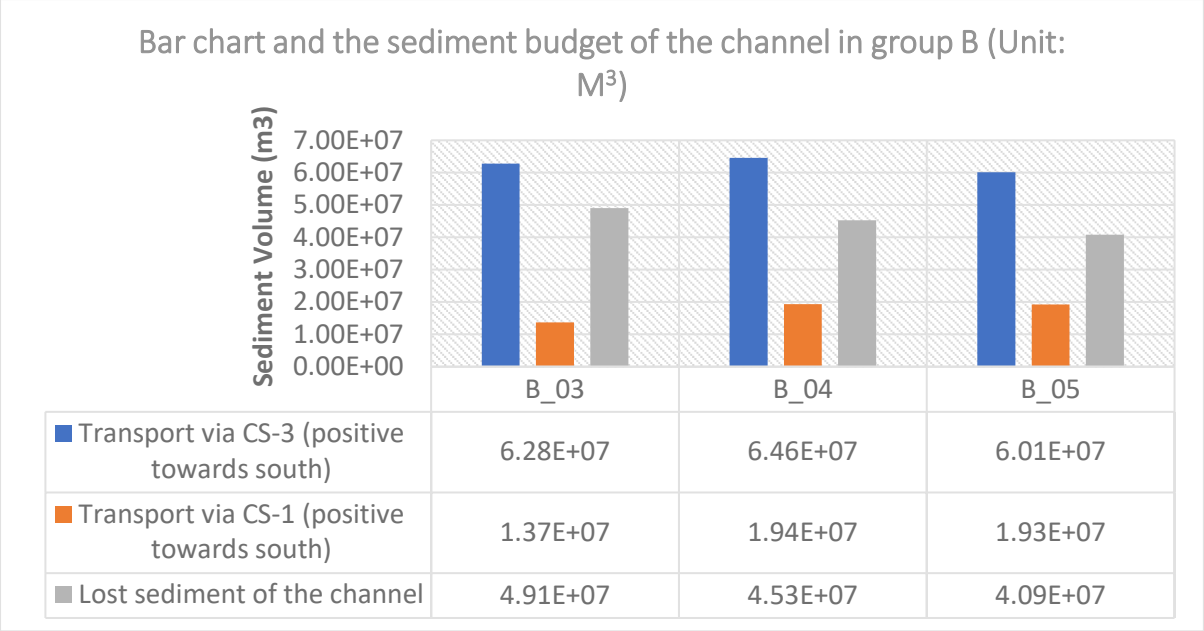

	B_03	B_04	B_05
Transport via CS-3 (positive towards south)	6.28E+07	6.46E+07	6.01E+07
Transport via CS-1 (positive towards south)	1.37E+07	1.94E+07	1.93E+07
Lost sediment of the channel	4.91E+07	4.53E+07	4.09E+07

Figure 21. The bar chart of the sediment budget of the channel in group B, with information on sediment volume attached.

The change in the volume of both non-cohesive sediment type on the ebb tidal delta is plotted in Figure 22. Over the simulated 20 years, there are increases in both volume of coarse sediment (250 μm) and fine sediment (100 μm) while the trends shows discrepancy. To be more specific, the volume change of coarse sediment is around 6.3E+07 m^3 and the difference between three scenarios are smaller than 3%. On the other hand, the change in volume of fine sediment increases up to 3.3E+07 m^3 after 12 years and then decrease to on average 2.0E+07 m^3 by the end of 20 years. Specifically speaking, B_03 experiences the most increase in fine sediment (2.2E+07 m^3) after 20 years, while B_04 and B_05 ends up at 1.8E+07 m^3, which is 22% less than B_03. Overall, the inconsistence on changes in coarse sediment on ebb tidal delta between different erodibilities is negligible while it is more significant in changes in fine sediment.

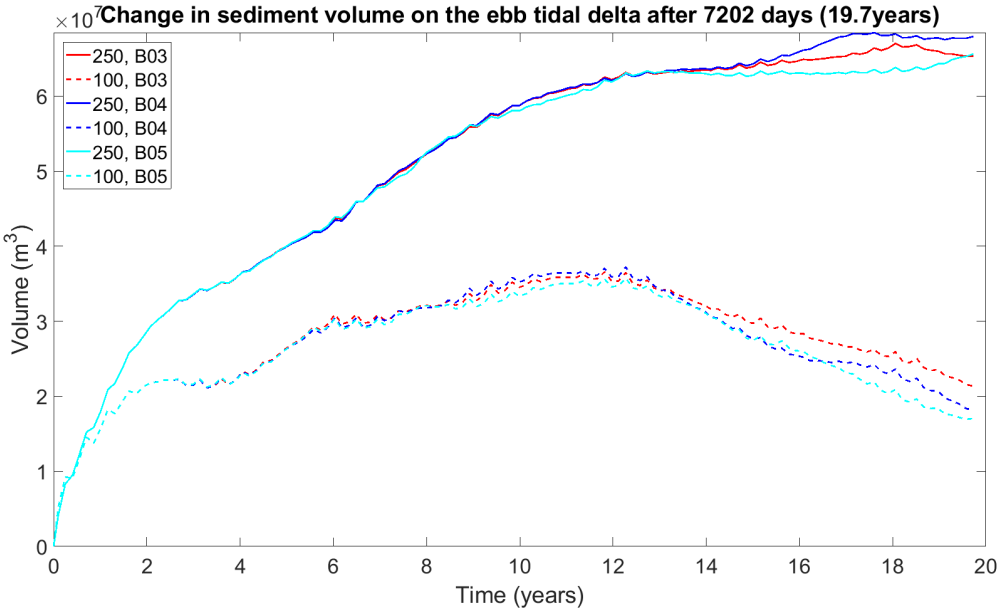

Figure 22. The change in sediment volume on the ebb tidal delta after 20 years simulation (Group B). Solid lines indicate the sediment with D50 = 250 μm and dashed lines indicate the sediment with D50 = 100 μm.

3.4 Group C: The effect of adding erosion-resistant patches on tidal inlet morphology

The scenarios in group C are listed in Table 4.

Table 4. The scenarios in group C.

Group C: to study the effect of adding erosion-resistant patches on tidal inlet morphology	
RUNID	Combinations of multiple erosion-resistant layers
C_01	No erosion-resistant layer
C_02	A uniform erosion-resistant layer at -20 m depth
C_03	A rectangular patch of erosion-resistant deposit located at the eastern part of the tidal channel at -13 m (See Figure 10)
C_04	The combination of C_02 & C_03 (See Figure 10)

3.4.1 Morphology

The comparison of morphology map within group C is shown in Figure 23. C_01 has the deepest main channel up to more than -30 meters because there was no erosion-resistant layer in the subsurface. In, C_02 the channel is shallower and wider than C_01 due to the presence of the uniform erosion-resistant layer at -23 meters. In C_03, the most part of the main channel is filled up by the rectangular patch of erosion-resistant layer. Subsequently, intertidal channels show distinctive patterns with C_01 and C_02, which are deeper, straighter and less bifurcated. In C_04, which is the combination of C_02 and C_03, the effect of erosion-resistant patch at -13 meters is still pronounced while the intertidal channel patterns is more similar with C_01 and C_02.

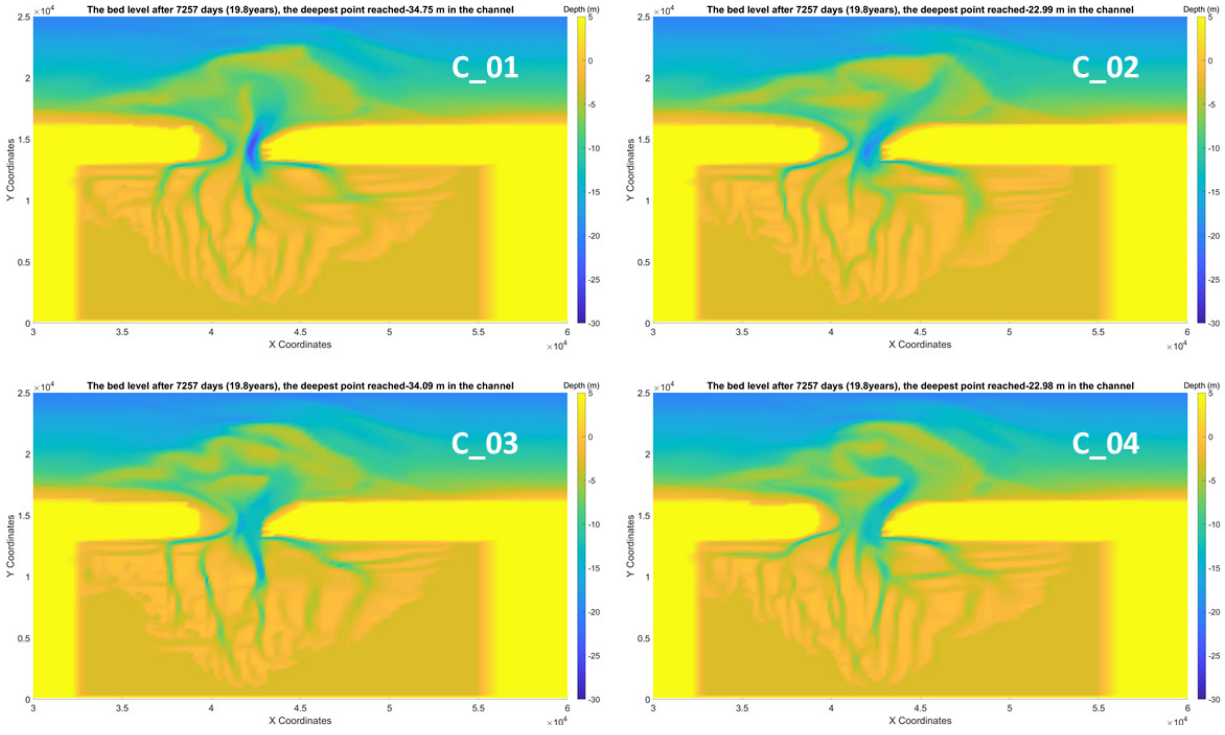

Figure 23. The comparison of morphology map between six scenarios in group C. (1) C_01 represents the scenario without erosion-resistant layers; (2) C_02 represents the scenario with a uniform erosion-resistant layer at -23 meters NAP; (3) C_03 represents the scenario with an erosion-resistant patch at -13 meters NAP, whose location was given in Figure 11; (4) C_04 represents the scenario combining C_02 & C_03.

3.4.2 Channel geometry

The comparison of the time stack plots of depth evolution in CS-2 in group C is shown in Figure 24. Due to the lack of erosion-resistant layers, the channel can migrate and incise freely into the subsurface reaching more than -30 meters NAP. Hardly any erosion occurred on the bank of eastern

barrier island. After adding a uniform erosion-resistant layer (C_02), the depth of the main channel is constrained to be above -23 meters. The 600 meters of the bank line on the eastern barrier island experienced erosion after 20 years. The sole presence of erosion-resistant patch is unable to constrain the channel depth at the first 14 years. However, after 14 years, the channel is limited to be above -13 meters. The erosion of the eastern barrier island starts earlier than C_01 and C_02. In C_04, which is the combination of C_02&C_03, the channel depth is initially constrained by the erosion-resistant layer at -23 meters NAP and then after 14 years, the channel depth is constrained by another layer at -13 meters NAP. The amount of erosion on the eastern barrier island does not differ much from C_03.

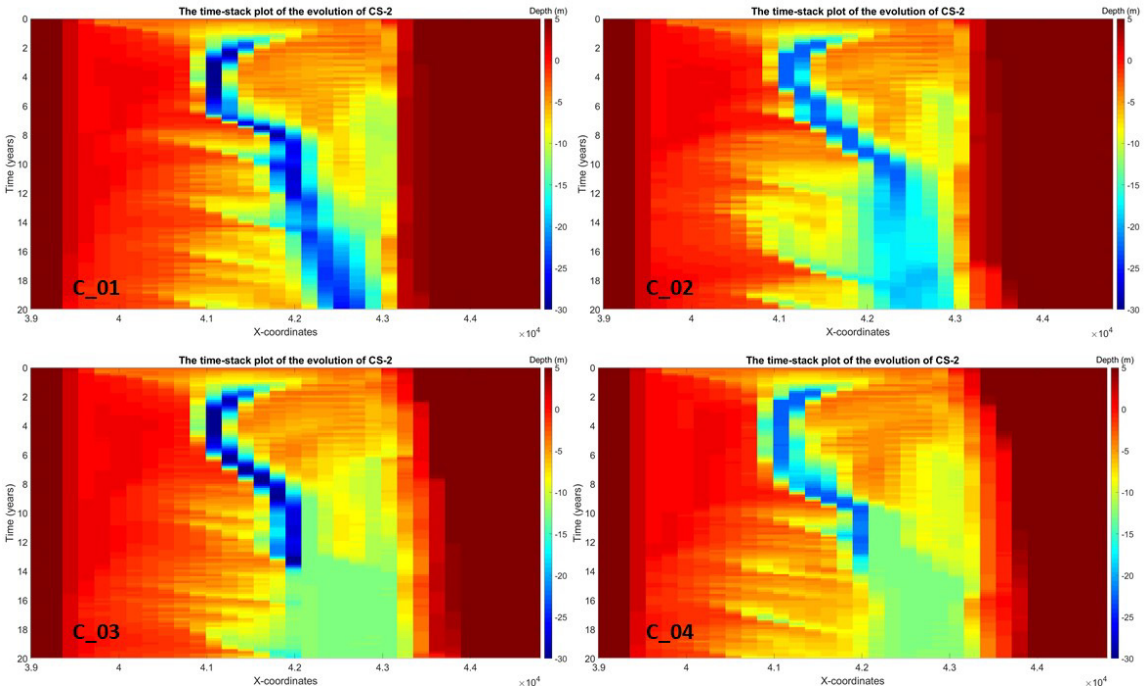

Figure 24. Comparison of time stack plots of depth evolution in CS-2 in Group C.

By looking at the evolution of channel profile of C_03 in the Figure 25, it can be seen that the thalweg was initially located at the western part of the channel, therefore it is not affected by the erosion-resistant patch. Then the thalweg gradually move towards east. When the channel encounters the erosion-resistant patch, the thalweg moves onto the terrace of erosion-resistant patch and stay on it for almost 5 years. In C_04, the process looks like the combination of C_02 and C_03. The channel was limited by the erosion-resistant layer at -23 meters at the first 13.5 year. When the channel migrates to the east, the channel is later affected by the erosion-resistant patch at -13 meters.

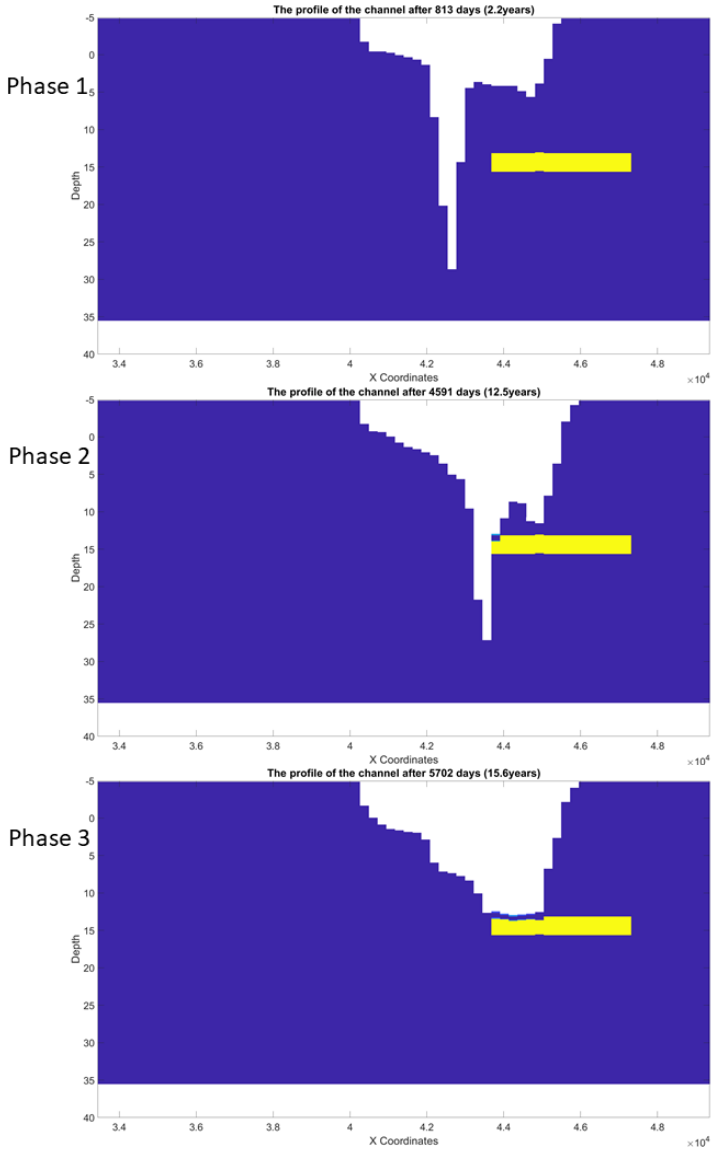

Figure 25. The evolution of channel profile of C_03. The yellow patch represents the erosion-resistant patch.

3.4.3 Sediment budget

Figure 26 plots the bar chart of the channel sediment budget in group C. Generally, there is not much difference in sediment budget for all four scenarios. This implies that adding erosion-resistant patches has limited influence on overall channel sediment budget after 20 years.

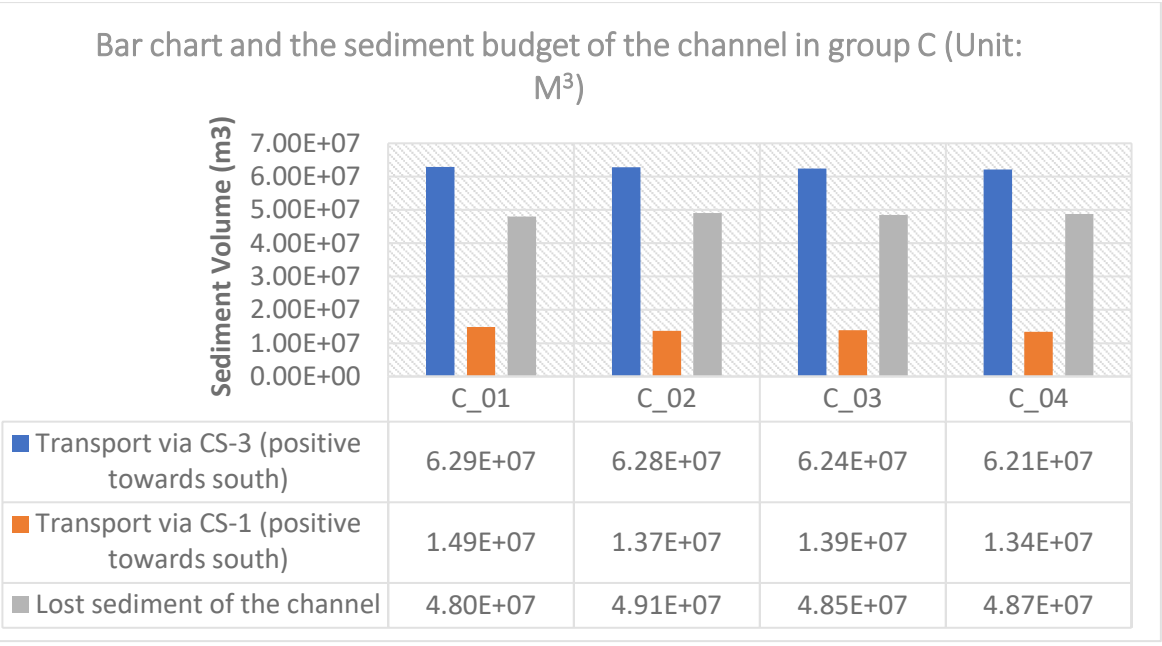

	C_01	C_02	C_03	C_04
Transport via CS-3 (positive towards south)	6.29E+07	6.28E+07	6.24E+07	6.21E+07
Transport via CS-1 (positive towards south)	1.49E+07	1.37E+07	1.39E+07	1.34E+07
Lost sediment of the channel	4.80E+07	4.91E+07	4.85E+07	4.87E+07

Figure 26. The bar chart of the sediment budget of the channel in group A, with information on sediment volume attached.

Turning to the change in sediment budget of the ebb tidal delta (Figure 27), the changes in volume of coarse sediment (250 μm) for these four cases are in the range from 6.4E+07 m^3 to 7.5E+07 m^3, among which the C_03 ranking the first and C_02 at last. It seems that after the presence of uniform erosion-resistant layer, there is less increase in coarse sediment volume (from C_01 to C_02, from C_03 to C_04). However, adding the erosion-resistant patch in the channel can enhance the deposition of coarse sediment on the ebb tidal delta (from C_01 to C_03, from C_02 to C_04). On the other hand, the effect of adding an erosion-resistant patch on the change in fine sediment volume on the ebb tidal delta is more ambiguous. C_01 and C_04 experience the most change, which is around 3.4E+07 m^3. However, in the separated scenarios, C_03 has an increase of 3.0E+07 m^3 and C_02 initially grows up to 3.3E+07 m^3 then declines to 2.0E+07 m^3.

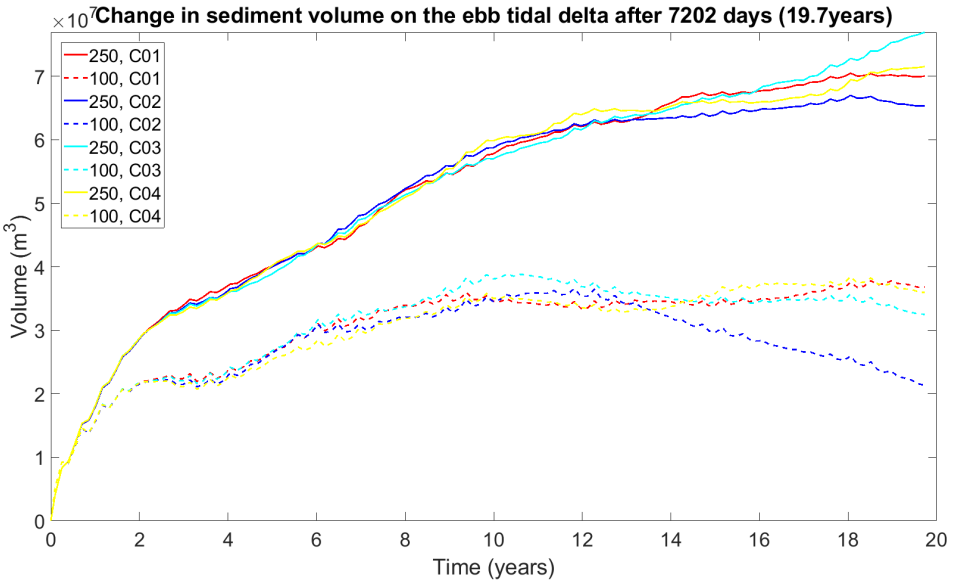

Figure 27. The change in sediment volume on the ebb tidal delta after 20 years simulation (Group C). Solid lines indicate the sediment with D50 = 250 μm and dashed lines indicate the sediment with D50 = 100 μm.

Discussion

4.1 Behavior related to depth and erodibility of erosion resistant layer

It was observed that in group A, there is less total sediment transport volume via CS-1 and CS-3 in simulations with a shallower erosion-resistant layer (Figure 17). One of the reasons could be related to smaller flow velocity in models with shallower erosion resistant layers. Since the elevation of erosion-resistant layer limits the depth of main channel, the shallower main channel is wider and does not focus the flow through a deep, narrow conduit, inducing more friction (de Swart & Zimmerman, 2009). Consequently, the flow velocity in the channel region is less so that less sediment is transported via the cross-sections. This also explains the decreased volume of fine sediment on ebb tidal delta as the erosion-resistant layers become shallower (Figure 18). Another potential reason is that the inlet acts as a sediment source for the ebb-tidal delta and the tidal basin, especially in the early stage of the simulation. A shallower erosion resistant layer would cause less available sediment supply.

In group B, after 20 years of morphological development, we observed that the channel orientation changed from the northeast to north or northwest in models with larger erodibility of the erosion-resistant layer (Figure 19). In addition, there are significantly more sediment transported via CS-1 in models with the increase in erodibility (Figure 21). These behaviors indicate that there is an increase in flow velocity. However, the depth of the main channel is -23 meters for all the cases in group B. However, in models with more erodible erosion resistant layers, the deepest part of the main channel is wider and the secondary channel in the west is also more pronounced and more active, increasing its capacity to contribute to the overall sediment transport.

4.2 Similar studies

Hijma (2017a) proposed a conceptual model on the effect of erosion-resistant layers on tidal channels, as mentioned in the introduction. Similarities were found between the modeled results with his conceptual model, as shown in Figure 28. The plots at the top left represents the channel profile before encounters the erosion-resistant layer (on the left) but it can also be used to demonstrate the profile when there is no erosion-resistant layer, which is in the same situation with the one on the top right. After adding an erosion-resistant layer at the bottom of the channel, Hjima (2017a) expected a shallower and wider and blunter profile. That is consistent with the result from A_06, with the erosion-resistant layer at -13 meters NAP. The channel depth is limited at -13 meters and the profile is flatter.

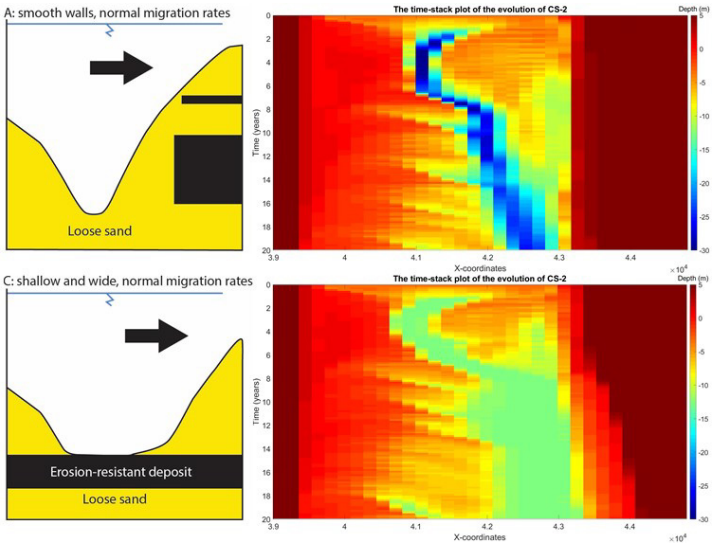

Figure 28. The conceptual model proposed by Hijma (2017a) on the left and the modeled result from this study on the right.

Comparing the modeled result with measured profile from Forzoni et al. (2018), there is a nearly vertical profile was formed on the eastern side of the channel and borehole data suggested that there are two hard layers at -23 meters and -13 meters respectively. In C_04, we set up the similar subsurface structure and the modeled result is comparable to measured results (Figure 29). the profile on the right is steep while the profile on the right is more gradual. This is because the erosion-resistant patch on the eastern side of the channel can prevent the channel from migrate towards east. However, due to the coarse grid resolution, the modeled profile is not smooth.

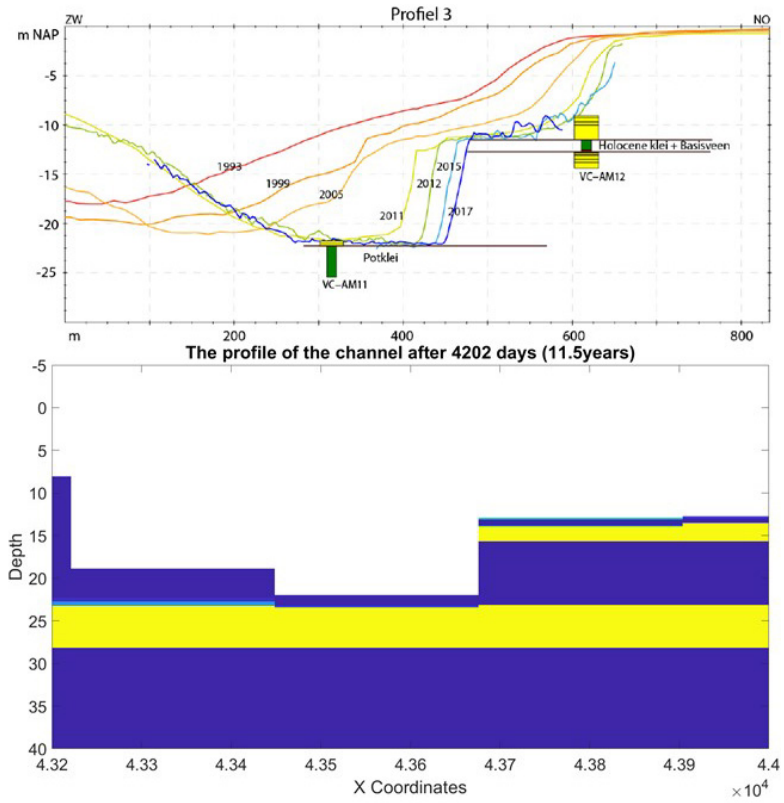

Figure 29. Top: the measured profile evolution at Ameland inlet from 1993 to 2017 with geological information. Bottom: the modeled channel profile at CS-2.

The model parameters used in this study are based on that proposed by Dissanayake et al. (2009) and therefore we compare our results with theirs. The most suitable scenario is the one without erosion-resistant layers (A_01&C_01) as there was also no such layer in their model. However, the results from Dissanayake et al. (2009) are the situation after 50 years while simulation A_01&C_01 only simulated 20 years of morphological development. The only simulation that did simulate 50 years in this study is the default case (A_04, B_01&C_02). We therefore compare the results from Dissanayake et al. (2009) to the scenario without erosion-resistant layers (A_01&C_01) as well as the default case (A_04, B_01&C_02) The main differences between the simulation from Dissanyake and our simulation are shown in Table 5.

Table 5. The difference in model setting between Dissanayake et al. (2009) and this study.

	Dissanayake et al.	A_01 & C_01	A_04, B_01 & C_02
Erosion-resistant layer	No	No	Yes
Simulation period	50 years	20 years	50 years
Sand fractions	Single - 200 µm	Multiple – 250 µm 100 µm	Multiple – 250 µm 100 µm
Inlet width	1 km	3.5 km	3.5 km
Morphological scale factor	100	40	40
Sediment transport formula	Van Rijn (1993)	Van Rijn (2007)	Van Rijn (2007)

In Figure 30(1a), the channel erodes to the depth more than -30 meters and the color scale is limited to 30m in depth, so it is not possible to know if their channel erodes deeper than 30. In our simulation without erosion resistant layers, the deepest part of the channel has approximately the same depth of 36 meters shown in Figure 30 (2a). In the results from Dissanyake et al (2009) the length of the channel that has the depth more than 20 meters is 10 km in length. while in both our simulations length of the part with depth more than 20 meters is significantly shorter. For the model which only simulated 20 years of morphological development this is to be expected as it has not had enough time to develop to this size (Figure 30 (2a)). For our simulation with erosion resistant layer the channel developed is also shorted, which could be because the presentence of the erosion resistant layer limits the volume of erodible sand which supplies the ebb delta, causing it to prograde slower. the differences in inlet width will also cause their model to experience larger flow velocities through the intel, causing sediment within the inlet to be moved towards the tidal basin and ebb delta at a faster rate and influencing the progradation speed. In our simulations the channel has more space to widen and shift within the inlet. This mean it will often shift sediment laterally instead of eroding deep into the subsurface. This will also decrease the rate of sediment supply to the ebb delta.

The orientation of the main tidal channel also differs in these two cases. The main channel orients towards northwest in their result while the direction of the main channel in Figure 30 (2a) is north-northeast. The reason can be twofold. On one hand, our case only ran until 20 years while their result is after 50 years. If we assume cyclic behavior for the channel orientation, then the moment at which the snapshot of the result is taken could cause significant differences in channel orientation. This is especially true of the progradation rate of the ebb deltas differs, as is the case here.

Turning to the volume change on the ebb tidal delta, in our case (2b), the sediment volume increased around 100 Mm^3 in 20 years as well and the increase slows down significantly at this point. The same happens for the scenario with erosion resistant layer where the ebb delta volume increase slows down and even reaches a maximum after 10 years, roughly coinciding with the time the channel reaches the erosion resistant layer. These are much smaller volumes that Dissanayake et. al (2009) records in their model with similar tidal conditions as our simulation (Figure 30 (1c), M2, M4). There are multiple hypotheses as to what causes this difference. Firstly, the inlet width is much narrower in their simulations. The narrow inlet will constrain the sediment availability so that less sediment can be transported onto the ebb tidal delta. Secondly, the difference in sediment grain size stored in the ebb delta. In their case this was 200µm and in our case the ebb delta mostly contains 250µm sands. The wave and tidal conditions in the sea will interact differently with these sediment classes. Lastly, due to their narrower tidal inlet, and potentially larger flow velocities, the longer, deeper, protruding channel which is one of the main features of the ebb delta also constitutes an erosive rather than depositional feature in the delta.

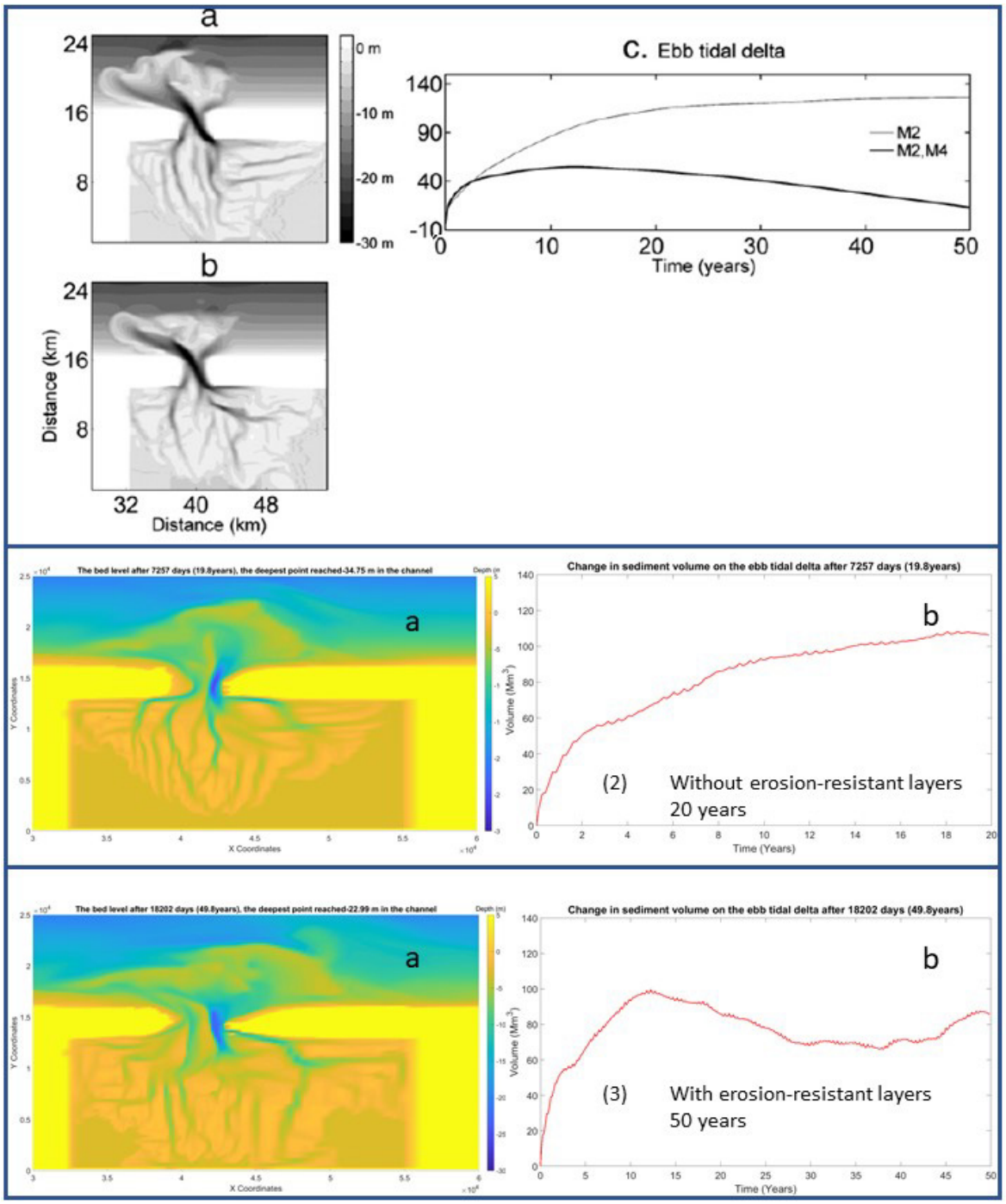

Figure 30. Block 1: Result from Dissanayake et al. (2009). (a) the morphology after 50 years simulation without tidal asymmetry (Only M2 tides); (b) the morphology after 50 years simulation with tidal asymmetry (M2 & M4); (c) the sediment volume of ebb tidal delta (Dissanayake et al., 2009). Block 2: Result from A_01&C_01, no erosion-resistant layers. Left: the morphology after 20 years. Right: The change in sediment volume on the ebb tidal delta after 20 years. Block 3: Result from A_04, B_01&C_02, with erosion-resistant layers. Left: the morphology after 50 years. Right: The change in sediment volume on the ebb tidal delta after 50 years.

Another similar study was done by Van der Wegen & Roelvink (2012), which is about the reproduction of estuarine bathymetry of Western Scheldt. Part of their sensitivity test was to investigate the influence of non-erodible layer on bathymetry evolution. It was found that adding the non-erodible layers makes the bathymetry fit better with the real case, especially for the shoal pattern in the channel (Van der Wegen & Roelvink, 2012). They concluded the presence of non-erodible layer can improve the quality of long-term prediction in Western Scheldt. However, their way to incorporate non-erodible layers is

different from this study. They simulate the non-erodible layers by setting the sediment availability at the grid cells, where the non-erodible layers locate, to zero. The erosion-resistant layers were parameterized using cohesive sediment in Delft3D by assigning extreme high critical shear stress for erosion. Compared with Van der Wegen & Roelvink (2012), the advantage of the model in this study is that the model is able to specify certain structure of the subsurface and it is able to assign variable erodibilities to erosion-resistant layers.

4.3 Model limitations and future study recommendations

4.3.1 Grid resolution

The grid size was set to be approximately 200m×150m in the area of most interest (channel region) and around 2000m×1800m at the domain boundaries. This grid resolution is not able to resolve channels in the tidal basin, whose width are in the order of 10^0 or 10^1 meters. This mismatch in scale can cause inaccuracy in the prediction of the tidal basin morphology and makes it meaningless to do investigations on detailed channel migration information in the tidal inlet. Furthermore, according to Hijma (2017a), the typical channel migration speed of tidal channels in the Ameland-region varies between 3 meters to 20 meters per year, so far less that size of our grid cells, which would therefore only be able to capture channel migration over 50-60 years. However, the larger wave heights assigned compared to annual averages can influence the rate of morphological development. The initial, flat channel bathymetry, far from an equilibrium situation with hydrodynamic conditions, can also cause an increased rate of development of the morphology, especially at the start of the simulation.

For future studies, the resolution at the interested area can be improved to 50m * 50m in order to capture the channel behavior over 20 years' time scale more accurately. In the meanwhile, the domain size at the distal boundaries can be decreased to maintain the approximately same computational speed.

4.3.2 Simulation period

Due to the length of the internship, all the model runs were set to have a simulation period of 20 years, except for the default one, which has a simulation period of 50 years. Based on the observation on the default simulation, the system seems to have a cyclic evolution with a certain period. The main channel starts to migrate to the west towards the end of the 50-years simulation. Adding and adjusting the properties erosion-resistant layer is likely to affect the cyclic period. Because the erosion-resistant layers can influence morphology of the inlet system and channel geometry, which can further affect the tidal prism. Moreover, there is a positive relationship between the tidal prism and the periods between successive shoal attachment (Ridderinkhof et al., 2016). It this case, after 20 years, there is a chance that the simulations were at different phases of their own cyclic behaviors, which for sure will bring discrepancies to the results and the analysis. In other words, the variance we found in each group cannot be fully attributed to the direct effect of the erosion-resistant layers.

This problem can be solved by lengthening the simulation period for all simulation and try to include at least one cyclic period. Then the results can be compared in the same phases of each simulations other than actual time points.

4.3.3 Lateral erosion

In reality, erosion occurs from the top and the side of the sediment body, as shown in panel a & b Figure 31. When there is shallower erosion-resistant patch above the uniform one with sand body in between, lateral erosion still occurs and will eventually form a profile indicated by the red curved line in panel b. In Delft3D, the amount of lateral erosion of a sediment column is calculated but then the model still takes sediment from the top layer rather than from the entire laterally exposed sediment stack. Consequently, this will bring contradiction between reality and model results.

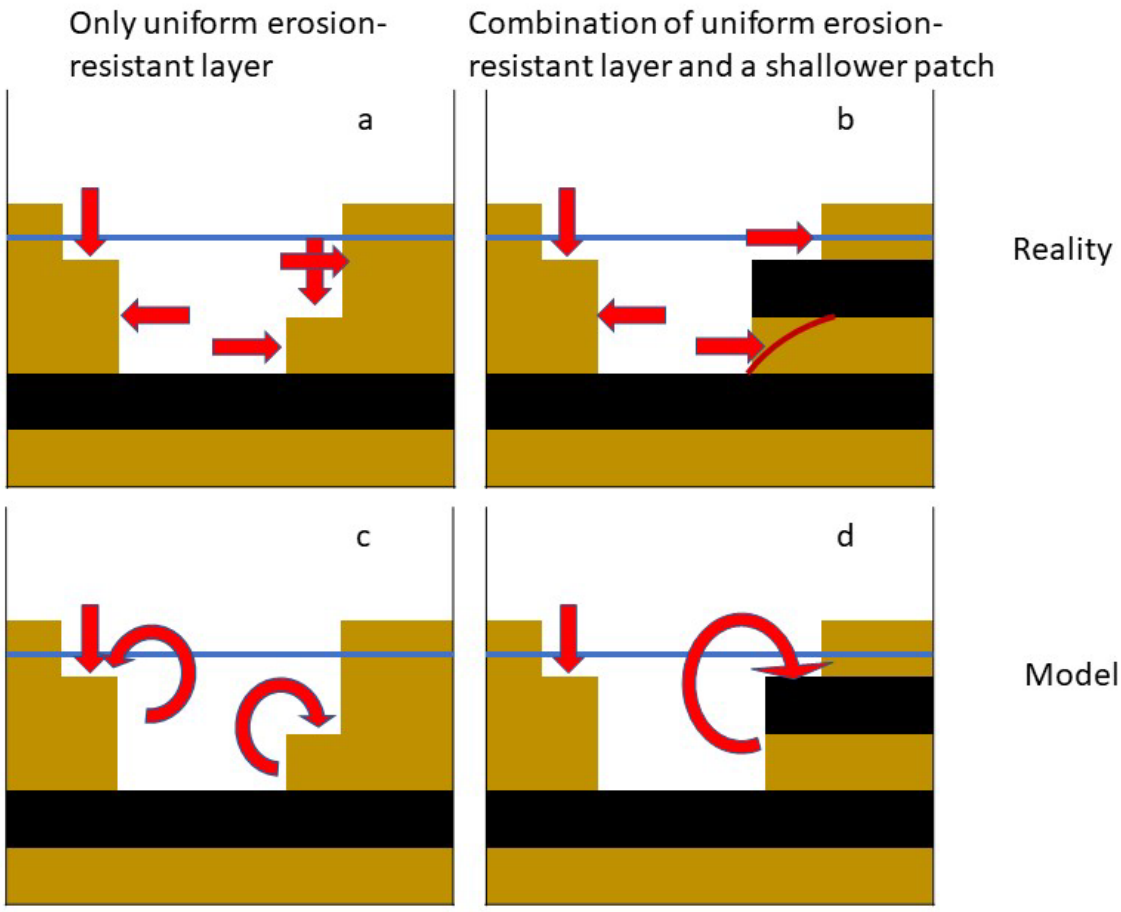

Figure 31. The schematized plot of the difference between erosion mechanism in reality and in the model. The brown color indicates the non-cohesive sediment, the black color indicates the erosion-resistant layers. The straight red arrow represents the location and the direction of erosion. The red curved arrow indicates that the erosion happens on the side while the model still takes sediment from the top layer of each sediment column. The red curved line illustrates the possible interface of the sediment after side erosion.

4.3.4 Analysis approach

The analysis in the study lacks quantitative method to describe the effect of erosion-resistant layers. This led to difficulties in result interpretation and most of them were qualitative statements. Besides, the objectives chosen in the analysis did not cut to the core of the influence which is induced by erosion-resistant layers. For example, as discussed before, the change in flow velocity can be one of the driving factors of the morphological difference between scenarios. Whereas the result is not presented in the report due to limitation of time.

Improvement can be made for future study that to use some quantitative parameters to describe the model results. For example, Brier Skill Score can be used to compare the model performance if there is measured data (Van der Wegen & Roelvink, 2012). In addition, to find the important variable for result analysis is also crucial for better result interpretation.

Conclusions

The study investigated the effect of erosion-resistant layers on evolution of tidal inlet morphology using a process-based model. Starting with a homogenous bathymetry, the model reasonably reproduced many of the features of the evolving morphology of Ameland using a schematized approach. The features reproduced include typical behaviors like cyclic evolution, shifting between 'one channel system' and 'two channels system', the development of ebb tidal delta and channels insides the tidal basin are reproduced by the model.

Adding a uniform erosion-resistant layer alters the system significantly, while the influence depends on the depth of erosion-resistant layer. Predominantly, the erosion-resistant layer prevents the channel from eroding deep into the subsurface and make the channel profile flatter. However, this influence declines as the erosion-resistant layer locates deeper in the subsurface. The adding of hard layers will decrease the amount of sediment transport from the sea to the channel as well as from the channel to the tidal basin, which is probably related to the decrease in flow velocity and in available sediment volume as discussed. In addition, more reduction was found via the cross-sections between sea & channel and channel & tidal basin which resulted in an increase in exported sediment from the channel. On the ebb tidal delta, scenario with deep erosion-resistant layers will induce more coarse sediment while scenario with shallow erosion-resistant layers behave the opposite. The amount of fine sediment deposited on the ebb tidal delta is less in all scenarios compared with the case without hard layers.

The erodibility of the erosion-resistant layers can also exert influence on tidal inlet morphology, which was examined by varying the critical shear stress for erosion. As the increase in erodibility, the channel is oriented more towards north and the channels insides the tidal basin can reach further. The effect of erodibility on sediment budget is pronounced. The increase in erodibility will increase the amount of sediment traveling from the sea to the channel so that the amount of sediment lost from the channel region is reduced. These behaviors indicated that there could be an increase in flow velocity via the channel which made the main channel straighter and more sediment transported from the sea to the channel. Exactly how the erodibility of erosion-resistant layer can affect flow velocity remains unclear and requires further investigation in future with adjusted. In particular, longer simulation times and slightly shallower erosion resistant layer, which interacts with the main channel more significantly, could help better constrain the influence of the erodibility on the morphological development Variance between scenarios in volume change of coarse sediment on the ebb tidal delta is negligible while fine sediment volume receives more influence.

Tidal inlet morphology can also be affected by adding erosion-resistant patches comparable to the latest subsurface configuration found for the Ameland inlet (Forzoni et al., 2018). The presence of the erosion-resistant patch at -13 meters will fill up the space where the main channel used to be located by hindering the channel to erode deeper. In addition, the intertidal channel will be shorter and less bifurcated with the presence of the erosion-resistant patch which can be attributed to the decrease in flow velocity. An interesting finding is that the patch is not constraining the channel depth until the 12.5th year. After that, the main channel migrated to the horizontal position of the patch and become limited by it. Not much influence was found on channel sediment budget. The presence of the erosion-resistant patch in the channel can enhance the deposition of coarse sediment on the ebb tidal delta. The influence on fine sediment volume is significant but hard to draw any regularities. However, in reality, the configuration of the subsurface encounters two very different erosion resistant layers, the shallower path probably being much more erodible than the underlying potclay layer. Detailed measurements of these layers' erodibilities are currently not available but would be an interesting addition to future investigations.

To sum up, an exposed erosion-resistant layer influences the evolution of tidal inlet morphology and the detailed influence is further depended on the depth, erodibility and special distribution of erosion-resistant patches. The result of each aspect is summarized in Table 6. Varying erodibility did not have impact on sediment budget of the ebb tidal delta and adding erosion-resistant patch at -13 meters did

not influence sediment budget of the channel in these simulations. However future simulations have been proposed to better investigate these aspects and more closely determine the effects of these parameter variations.

Table 6. The concluded effect of erosion-resistant layers on four aspects of the Ameland inlet system. The checkmark means the property of erosion-resistant layers can affect the corresponding aspect while the cross mark represents the opposite.

	Morphology	Channel geometry	Sediment budget of the channel	Sediment budget of the ebb tidal delta
Depth	✓	✓	✓	✓
Erodibility	✓	✓	✓	✗
Adding erosion-resistant patches	✓	✓	✗	✓

For future studies, the resolution of the grid system should be improved, e.g. 50m * 50m in the interested area, so that the evolution of channels can be better reproduced. The simulation period should be lengthened to at least 50 years thereby the system can reach an equilibrium or dynamic equilibrium state which would reduce model noise and make the result analysis more reliable. Smaller domain should also be implemented on the condition that the future study would focus more on mechanism of erosion-resistant layers rather than reproduce the Ameland inlet in the model. In addition, more quantitative analysis throughout the morphological development (not only at the end of the morphological evolution) should be used to give reasonable explanation to the effect of erosion-resistant layers.

Reference

Booij, N. R. R. C., Ris, R. C., & Holthuijsen, L. H. (1999). A third-generation wave model for coastal regions: 1. Model description and validation. Journal of geophysical research: Oceans, 104(C4), 7649-7666.

Cheung KF, Gerritsen F, Cleveringa J (2007) Morphodynamics and sand bypassing at Ameland Inlet, the Netherlands. J Coast Res 23(1):106–118

Cleveringa, J., Geleynse, N., (2017). Shapefiles historische ligging geulen buitendelta's van Waddengebied, Zeeland en Zuid-Holland. Arcadis report

De Glopper, R.J., (1967): Over de bodemgesteldheid van het Waddengebied. - Van Zee tot Land, 43, 67 pp. (with English summary).

Deltares (2018). Delft3D-FLOW User Manual (Version 3.15.54312). Delft, The Netherlands: Deltares.

De Swart, H. E., & Zimmerman, J. T. F. (2009). Morphodynamics of tidal inlet systems. *Annual review of fluid mechanics*, *41*, 203-229.

Dissanayake, D. M. P. K., Roelvink, J. A., & Van der Wegen, M. (2009). Modelled channel patterns in a schematized tidal inlet. *Coastal Engineering*, *56*(11-12), 1069-1083.

Dissanayake, D. M. P. K., Ranasinghe, R. W. M. R. J. B., & Roelvink, J. A. (2012). The morphological response of large tidal inlet/basin systems to relative sea level rise. *Climatic change*, *113*(2), 253-276.

Elias, E. P., & Hansen, J. E. (2013). Understanding processes controlling sediment transports at the mouth of a highly energetic inlet system (San Francisco Bay, CA). *Marine Geology*, *345*, 207-220.

Engelund, F., Hansen, E., 1967. A Monograph on Sediment Transport in Alluvial Streams. Teknisk Forlag, Copenhagen.

Forzoni, A., Hijma, M.P., Vermaas, T., (2018). Geologie en morfodynamiek getijdengeulen. Deltares report 11202190-001-ZKS-0002, 26 pp.

Hijma, M.P., (2017a). Geology of the Dutch Coast. Deltares report 1220040-007-ZKS-0003, 43 pp.

Hijma, M.P., (2017b). Tidal-channel migration between 1997-2014 in relation to the local build-up of the subsurface, The Netherlands. Deltares report 11200538-004-ZKS-0003, 40 pp.

Holthuijsen, L. H. (2010). *Waves in oceanic and coastal waters*. Cambridge university press.

Israel CG, Dunsbergen DW (1999) Cyclic morphological development of the Ameland Inlet, the Netherlands. In: Proceedings IAHR Symposium on river, coastal and estuarine morphodynamics, Department of Environmental Engineering, University of Genoa, pp 705–714

Lenstra, K. J., Pluis, S. R., Ridderinkhof, W., Ruessink, G., & van der Vegt, M. (2019). Cyclic channel-shoal dynamics at the Ameland inlet: the impact on waves, tides, and sediment transport. *Ocean Dynamics*, *69*(4), 409-425.

Lesser, G. R., Roelvink, J. V., Van Kester, J. A. T. M., & Stelling, G. S. (2004). Development and validation of a three-dimensional morphological model. *Coastal engineering*, *51*(8-9), 883-915.

Partheniades, E. (1965). Erosion and deposition of cohesive soils. Journal of the Hydraulics Division, 91(1), 105-139.

Postma, H., (1954): Hydrography of the Dutch Wadden Sea. - Arch. Néerl. Zool., 10, p.405-511.

Postma, H., (1961): Transport and accumulation of suspended matter in the Dutch Wadden Sea. - Neth. J. Sea Res., 1, p. 148-190.

Ridderinkhof, H. (1988a). Tidal and residual flows in the Western Dutch Wadden Sea I: numerical model results. Netherlands Journal of Sea Research, 22(1), 1-21.

Ris, R. C., Holthuijsen, L. H., & Booij, N. (1999). A third-generation wave model for coastal regions: 2. Verification. *Journal of Geophysical Research: Oceans*, *104*(C4), 7667-7681.

Roelvink, J. A. (2006). Coastal morphodynamic evolution techniques. Coastal engineering, 53(2-3), 277-287.

Roelvink, J.A., Van der Kaaij, T., Ruessink, B.G., 2001. Calibration and verification of large-scale 2D/3D flow models, Phase 1, Delft Hydraulics report, Z3029.11.

Sassi, M., Duran-Matute, M., van Kessel, T., & Gerkema, T. (2015). Variability of residual fluxes of suspended sediment in a multiple tidal-inlet system: the Dutch Wadden Sea. *Ocean Dynamics*, *65*(9-10), 1321-1333.

Sha LP (1989) Variation in ebb-delta morphologies along the West and East Frisian Islands, The Netherlands and Germany. Mar Geol 89(1):11–28

Van der Spek, A.J.F., (1994). Large-scale evolution of Holocene tidal basins in the Netherlands. Ph.D.-thesis, Utrecht University, Utrecht.

Van der Spek, A. J. F. (1996). Holocene depositional sequences in the Dutch Wadden Sea south of the island of Ameland. Mededelingen Rijks Geologische Dienst, 57, 41-69.

Van der Wegen, M., & Roelvink, J. A. (2012). Reproduction of estuarine bathymetry by means of a process-based model: Western Scheldt case study, the Netherlands. Geomorphology, 179, 152-167.

Van kessel, T., Boer, A., S., Van der Werf, J., Sittoni, L., Van Prooijen, B., Winterwerp, H., Bed module for sand-mud mixtures. Deltares report 1200327-000-ZKS-0013, pp 111.

Van Rijn, L.C., 1993. Principles of Sediment Transport in Rivers, Estuaries and Coastal Seas. AQUA Publications, the Netherlands.

Van Rijn, L.C. (2007a). Unified View of Sediment Transport by Currents and Waves. I: Initiation of Motion, Bed Roughness, and Bed-Load Transport. Journal of Hydraulic Engineering, 133, 649-667.

Van Straaten, L.M.J.U. & Kuenen, Ph.H., (1957): Accumulation of fine grained sediments in the Dutch Wadden Sea. - Geol. Mijnbouw, 19, p. 329-354.

Appendix

The result of sensitivity tests is listed here. The result of each sensitivity test is compared with the default case.

Selection of the transport formula

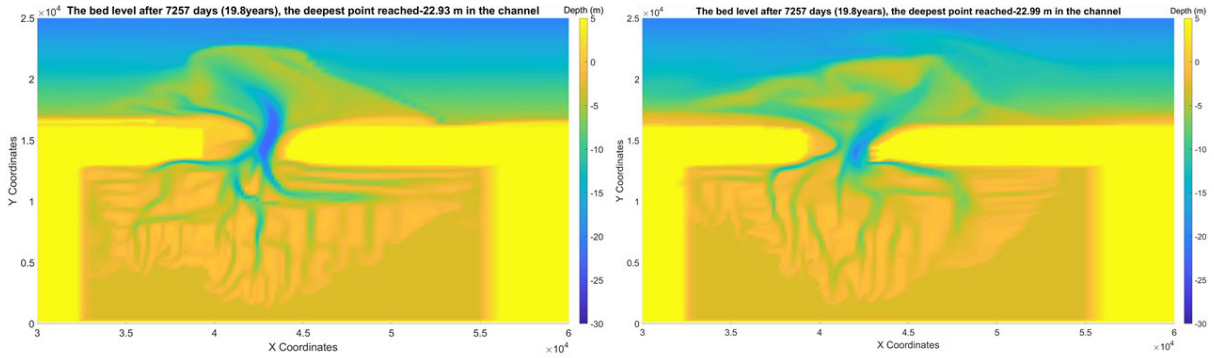

Figure 32. The comparison of morphological map between different sediment transport formula.

Based on Figure 32, the part of the channel reaching -23 meters is significantly larger using Van Rijn (1993) than using Van Rijn (2007). The main channel orients towards northwest and there is more deposition on the western part of the inlet region when using Van Rijn (1993). In addition, the secondary channel of the inlet is not visible and the channels inside the tidal basin are more perpendicular to each other when using Van Rijn (1993). Generally, Van Rijn (2007) produces morphology more similar to what is observed in reality.

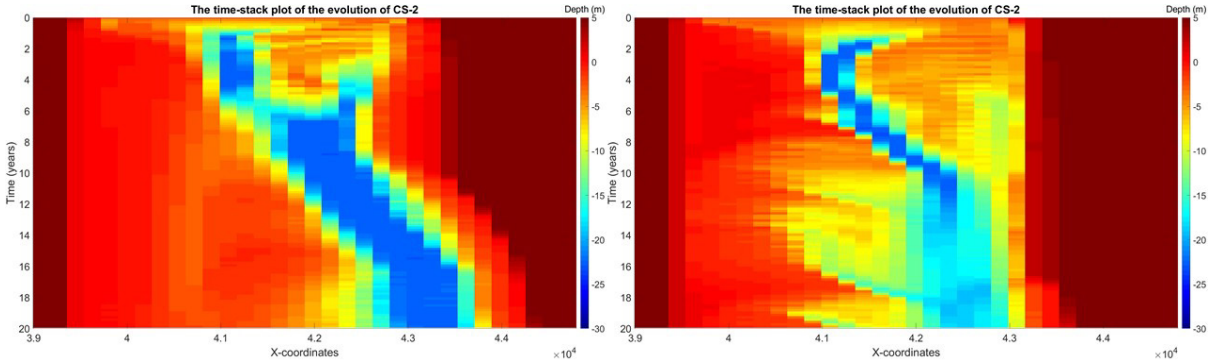

Figure 33. The comparison of time stack plot of channel profile evolution at CS-2 between different sediment transport formula.

As seen in Figure 33, similar to what is observed in the morphological map, the main channel is wider using Van Rijn (1993) and depth basically stays at -23 meters using Van Rijn (1993) while the channel can be deposited back to -15 meters again using Van Rijn (2007). Besides, more deposition on the western part of the inlet and more erosion on the eastern barrier island occurs.

Given the performance, Van Rijn (2007) was chosen in this study as the sediment transport formula.

Selection of the representative diameter of suspended sediment (Iopsus)

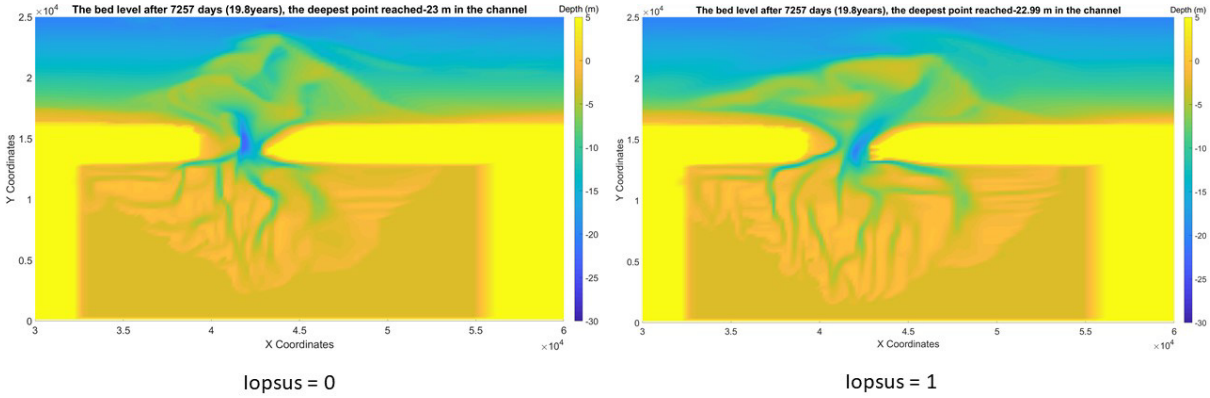

Figure 34. The comparison of morphological map between different representative diameter of suspended sediment (Iopsus).

When Iopsus = 0, the channel on the west part of the inlet is the deeper than the other channel on the east (Figure 34). Moreover, the intertidal channel is less developed if Iopsus equals zero (Figure 34). Given the performance, Iopsus was set to 1 in this study.

Selection of morphological time scale factor (MORFAC)

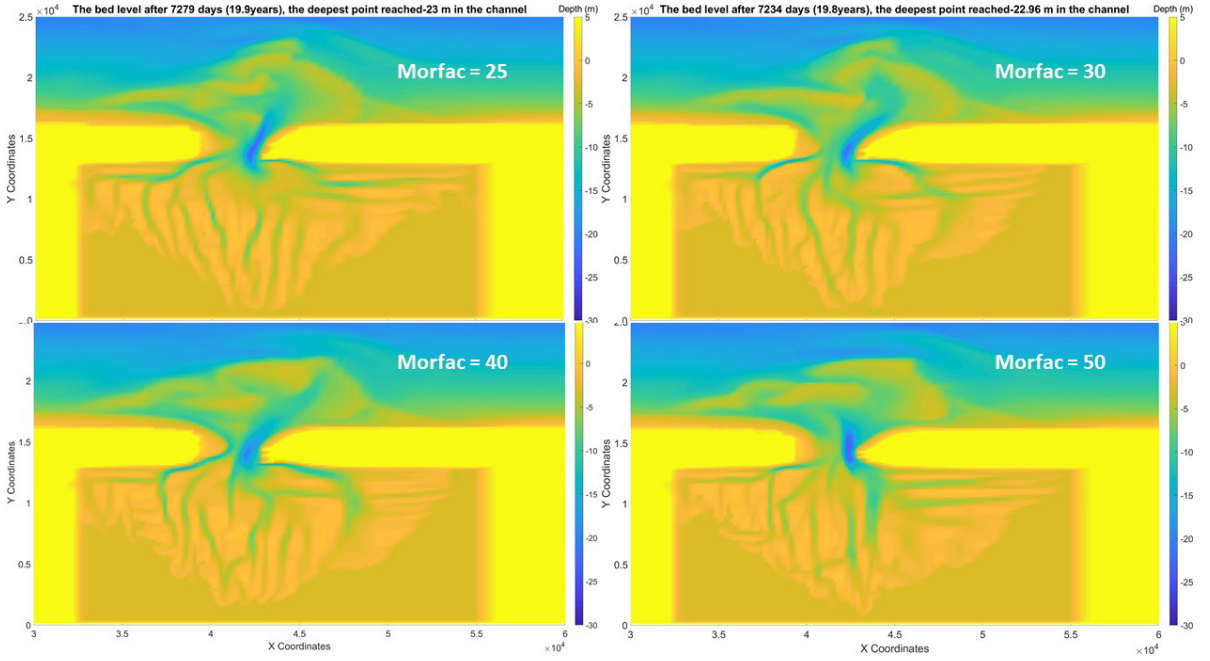

Figure 35. The comparison of morphological map between different morphological time scale factor (MORFAC).

When Morfac = 25, a northeast oriented channel was produced (Figure 35). The simulation with Morfac = 30 &40 performed similarly while the simulation with Morfac = 50 produced a north oriented channel. The rest of the features in system shows no significant inconsistence between 25, 30 and 40. Therefore, 40 was chosen for Morfac in this study.

Selection of dry cell erosion factor (ThetSD)

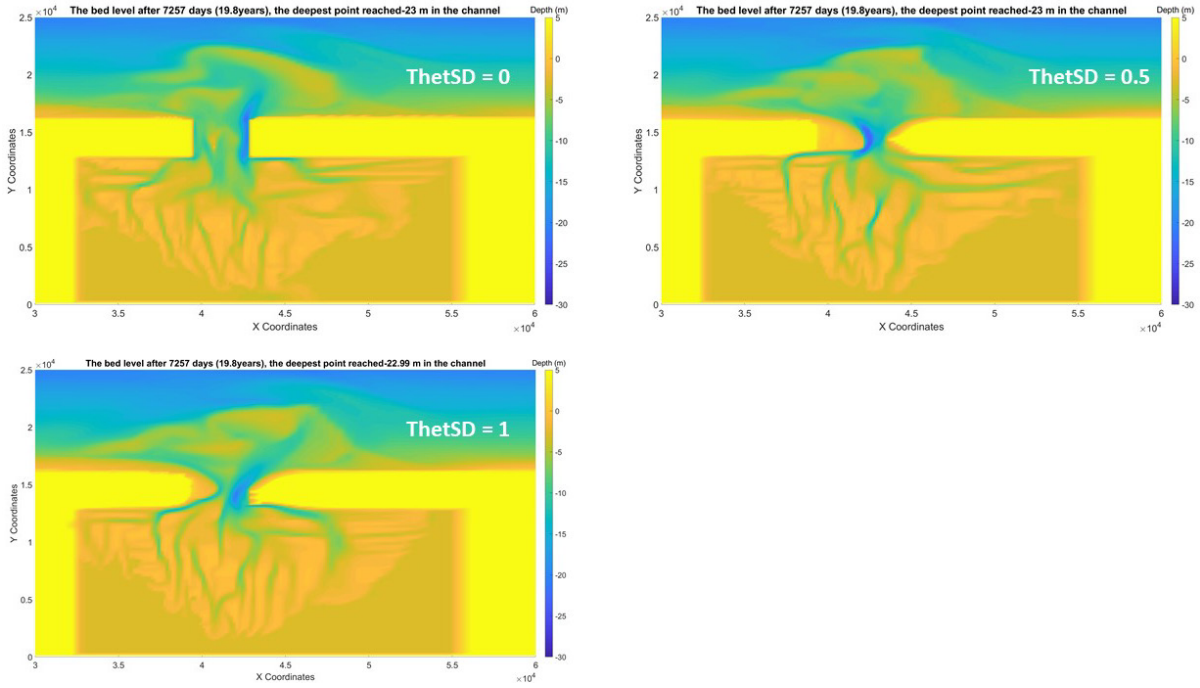

Figure 36. The comparison of morphological map between different dry cell erosion factor (ThetSD).

The comparison of morphological map for the selection of dry cell erosion factor is shown in Figure 36. When ThetSD was set to 0, there was no erosion on the bank of both barrier islands, because the erosion of the dry cells is switched off. Even through there was a deep channel on the side of the bank, as seen in Figure 36, no lateral erosion of the dry cells would occur. When ThetSD was to 0.5, we can see there are some erosion on the eastern barrier island. However, the main channel located at the western part of the inlet in this case. When ThetSD is 1, the main channel located at eastern part of the inlet, which is more similar to the morphology in reality.

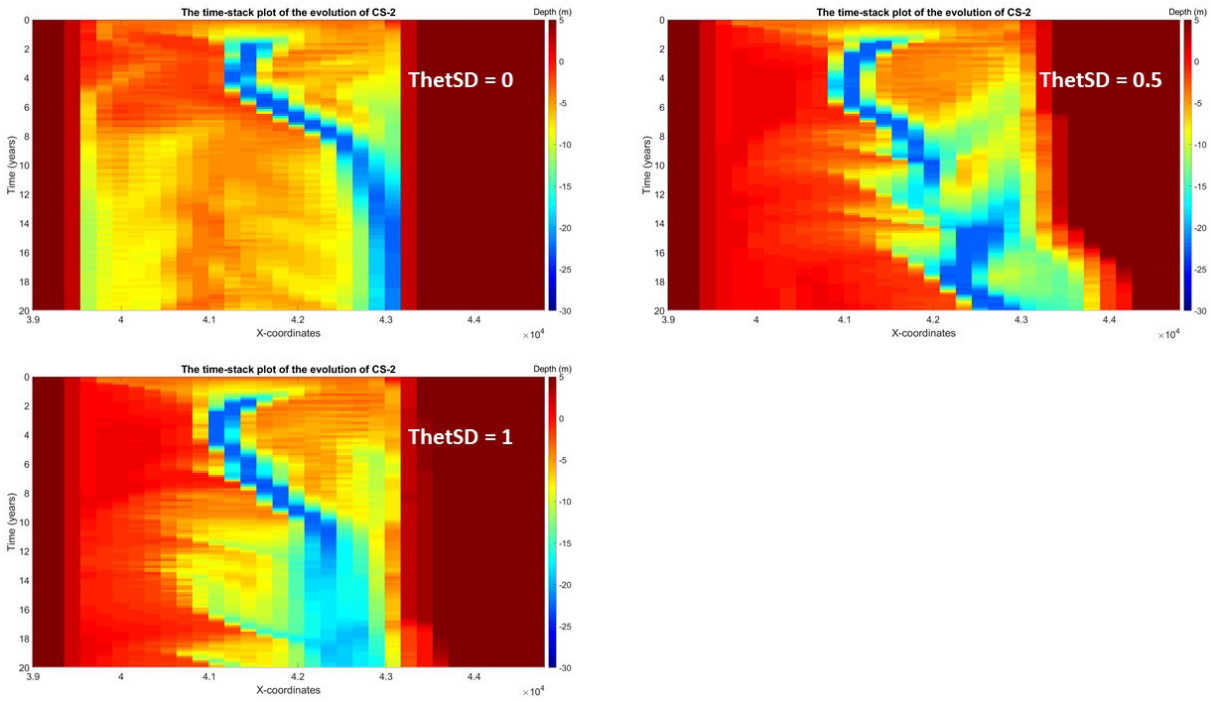

Figure 37. The comparison of time stack plot of channel profile evolution at CS-2 between different dry cell erosion factor (ThetSD).

Based on Figure 37, we can see that the smaller ThetSD is, the narrower would the main channel be. In other words, larger ThetSD tend to produce a flatter profile.

Given the model performance, the dry cell erosion (ThetSD) was set to 1 in this study.